Development of a cost efficient wind turbine blade for low wind speeds

J.L. van der Walt

orcid.org/0000-0001-9734-531X

Dissertation accepted in fulfilment of the requirements for the degree *Master of Mechanical Engineering* at the North-West University

Supervisor: Mr JD Human

Graduation: October 2020

Student number: 22698965

ACKNOWLEDGEMENTS

Wynand van der Wateren and Olivia Steyn for their friendship, support and advice during my undergraduate and postgraduate studies, which helped and motivated me throughout my years at university.

Dr Jan Janse van Rensburg, for his inspiration and guidance in his personal capacity during my academic career.

My parents, for their continuous encouragement to do more and be better, and by example showed me that a good education is a key to many doors. Thank you for supporting and funding my endeavours so that I may be where I am today, nothing would have been possible without you.

Our Lord God, for the opportunities, abilities, and people who have been part of my journey.

I, **Louis van der Walt,** declare that this report is a presentation of my own original work.

Whenever contributions of others are involved, every effort was made to indicate this clearly, with due reference to the literature.

No part of this work has been submitted in the past, or is being submitted, for a degree or examination at any other university or course.

Signed on the 18th day of November 2018, in Potchefstroom.

JL VAN DER WALT

ABSTRACT

With the growth of renewable energy in recent decades, innovative methods of power production are being researched to reduce humanity's dependency on finite- and pollution prone fossil fuels. In order to expedite the shift toward renewables as the primary source of global energy, the manufacturing and production cost of components in renewable power production must be reduced.

When considering the cost of producing wind turbine rotors and utilising these wind turbines in areas with low wind speeds (conventionally deemed unfeasible areas for wind farms), it is challenging to justify the use of wind energy. By lowering the manufacturing cost of the rotor blades and redesigning the blade characteristics for low wind speeds (such as those found in South Africa's inland regions), the production cost of energy may be lowered, thus increasing its feasibility as a power generation method.

This study investigated the use of rotational moulded polyethylene and a redesign of the rotor for low wind speeds such as those found in Potchefstroom, in South Africa's North-West province. By integrating the aerodynamic and structural design processes and determining the ideal design wind speed to serve as the base for the design, the blade was increased in length until a maximum size was reached that would satisfy the conditions for safety factors without any internal reinforcement.

The study used a blade element momentum theory-based aerodynamic design, and fed the blade-, environmental-, and airfoil characteristics into a beam-theory based structural model. Subsequently, the blade was increased in size until it could no longer withstand the region's simulated gust-wind conditions. The aerodynamic model was verified and validated by comparing the blade's predicted performance with results of a similar wind turbine blade's experimental testing.

Using the parameters and loads obtained from the acronymic model the beam-theory based structural design was verified by using a finite element method software package. The software's capabilities were then compared with real-world testing done on similar structures.

The integrated design model may be used for any environmental conditions or regions, and will provide an accurate prediction of an optimised rotor blade design and its performance.

Keywords: *Wind Turbine, Renewable Energy, Rotor Blades, Rotational Moulding, Low Wind Speed*

TABLE OF CONTENTS

LIST OF TABLES

LIST OF FIGURES

CHAPTER 1 INTRODUCTION

1.1. Background

Throughout history, wind has been harnessed by various cultures to, for instance, grind corn or pump water with crude wind mills. Today is no different with modern wind turbines that allow us to produce energy and with the ever-increasing focus on renewable energy, wind energy in particular has been a major focus of development.

South Africa currently faces electricity shortages and has, subsequently, invested heavily in renewable energy. The country placed fourth in 2014 by its share of annual GDP (gross domestic product) invested in renewable energy (REN21, 2014). The rapid growth in the renewable energy sector is illustrated by the development of a number of wind farms in various regions in South Africa and, since wind energy is dependent on environmental factors such as wind speed and wind availability, the coastal areas of the Western and Eastern Cape provinces has shown fair wind potential and preference for these developments (Caboz, 2018). The wind farms already in operation in these areas, have a total rated capacity of around 1000MW, or 2% of national power production (DoE, 2015).

Consequently, the wind energy industry should become more financially competitive regarding alternative renewable energy industries in both the South African public and private sectors. This makes wind energy an important area for innovation and development.

1.2. Problem statement

The private sector increasingly uses renewable energy sources to operate independently from the expensive and irregularly supplied electricity provided by South Africa's national power grid (Scholtz *et al.*, 2017). However, the cost per energy unit of smaller wind energy sources does not compare favourably with solar energy sources (Scholtz *et al.*, 2017) due to wind energy being notably more expensive and unreliable than installing small to medium capacity solar power infrastructure. The irregular supply of wind and the low average wind speed found in most regions of South Africa make the cost of wind energy per unit energy in South Africa high and unattractive for investment. However, reducing the cost of wind energy per unit energy, through a new design approach of the turbine – based on low wind speeds – and by using rotational moulding in the manufacturing of the rotor blades, may counteract the costs associated with conventional composite material layering methods.

1.3. Objective and scope

The objective of this research project is to design wind turbine blades with an innovative optimisation approach aimed at producing maximum annual power output at minimum cost.

This objective may be accomplished by designing and optimising wind turbine blades suited for weather conditions in South Africa, and by using rotational moulding in the manufacturing process to reduce costs. An existing airfoil profile is utilised in the design process. Ultimately, the goal is for the design wind speed to maximise the annual power output of the rotor as applicable to the low wind speeds of inland South Africa.

The structural and aerodynamic designs are conducted with the aid of software in order to optimise the blade geometry and profile for the characteristics of the rotationally moulded process and material used. The structural integrity of the blade serves as the limiting factor in the maximum length of the blades, with the blades being hollow – as per the manufacturing method – and having no internal support. The manufacture and experimental testing of the rotor does not form part of this study.

CHAPTER 2 LITERATURE REVIEW

This chapter provides the literature associated with the procedures, methods and information relevant to wind turbine rotor design.

2.1. Introduction

Historically, wind has been utilised as a power source for centuries. It initially took the form of windmills constructed from basic materials that could harness wind to pump water or to grind grain. By the 19th century, fossil fuels replaced alternative wind-based energy production, partly due to the inefficient and cumbersome designs of early wind turbines. With the development of advanced materials in the 20th century, such as composites and polymers, the wind energy industry underwent a resurgence and is currently being used to a great extent to generate electricity (DoE, 2015).

Modern wind turbines are generally divided by the axis of the rotation, either horizontally or vertically.

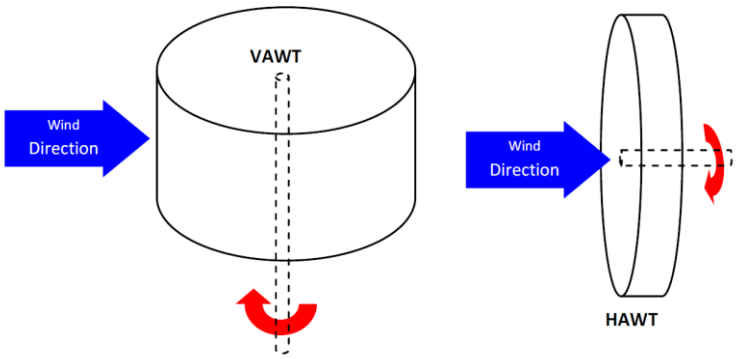

Figure 1: Wind turbine configurations (Schubel & Crossley, 2012:3426)

The concept of Vertical Axis Wind Turbines (VAWTs) relies on the wind arriving at a right angle to the turbine's rotational axis, as is the case in classic water wheels. This design is advantageous as it allows for the gearbox and generator to be placed on the ground, making it more accessible for maintenance and thus also circumventing the need for a yaw mechanism. In contrast to these advantages however, this method has much lower efficiency ratings. By placing the rotor close to the ground, the amount of wind that can be harnessed is also lower because wind speed increases with altitude due to the surface friction on ground level (DNV/Risø, 2002).

A Horizontal Axis Wind Turbine (HAWT) is the conventional design configuration. These turbines are designed to function when facing into the wind, so that the wind direction and axis of rotation

is parallel to one another. HAWTs are further divided into having either upwind or downwind rotors. Upwind rotors face the wind directly, the advantage being that the rotor avoids the wind shade from the tower and nacelle. Downwind rotors face away from the wind, letting it strike the tower and nacelle before passing through the rotor. This design allows for the omission of a yaw mechanism that keeps the rotor facing the wind, since the rotor may freely rotate to passively follow the wind direction. However, as the effective wind speed is hampered by the tower and nacelle, the effectiveness of this configuration is lower, and may give rise to higher loads on the rotor blades (DNV/Risø, 2002).

2.2. Modern wind turbine components

The production of electrical power from wind energy is dependent on the turbine's rotor design. This includes all the components that make up a wind turbine, from the tower's height to the rotor blade's shape. To extract the kinetic and potential energy of wind to produce electricity, modern wind turbines consist of various components, as shown in Figure 2.

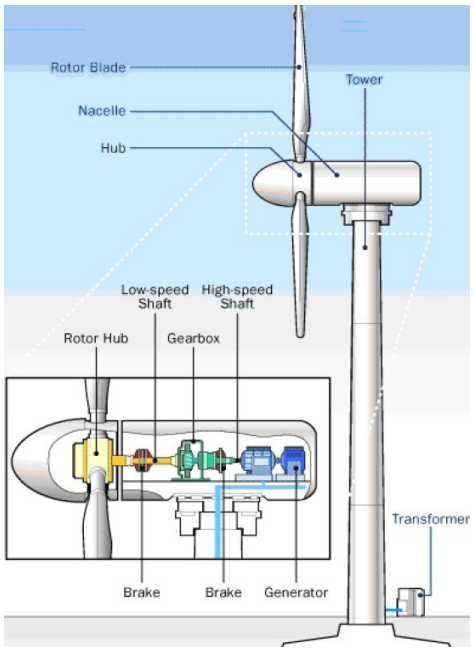

Figure 2: Wind turbine components (Al-Shemmeri, 2010:22)

The rotor blades component has the greatest impact on power generation. The rotor harnesses the wind, allowing the kinetic energy in the wind to be converted into electricity. The design of the blades is determined by the number of blades on the rotor and material used to manufacture these blades (RAENG, 2014b).

The number of blades is determined by the financial constraints regarding the blades' manufacturing, the visual appeal, desired efficiency and noise generation. These and other

factors determine the final decision of how many blades will be used. However, conventional designs of wind turbines usually make use of two or three blades (RAENG, 2014b).

The material used in the manufacturing process is selected by considering the strength-to-weight ratio, fatigue life, flexibility, and cost. The most commonly used materials include glass/polyester ply and laminate, glass/epoxy ply, and wood/epoxy laminate (RAENG, 2014b).

2.3. Estimating the power of wind

The amount of power that may be harnessed from wind is usually estimated by using calculations based on the conservation of momentum and conversion of energy to serve as a rough estimation of the expected power output of a wind turbine.

2.3.1. Correlation between wind speeds and power output

Wind turbines are designed for certain wind speeds. The following concepts related to wind speed and turbine design should be defined before commencing with the discussion of this study's objectives. The *cut-in speed* is the lowest wind speed that can overcome the inherent torque of the turbine and which can turn the rotor (WindPower Progam, 2018). The *cut-out speed* is the highest wind speed that the turbine can safely be exposed to. The turbine is braked or the rotor blades stalled whenever this wind speed is exceeded (WindPower Progam, 2018). The *rated output power* is the power that the generator will produce when reaching its optimum wind speed and it is known as the *rated output wind speed* (WindPower Progam, 2018).

Figure 3 below illustrates how the power output varies with wind speed.

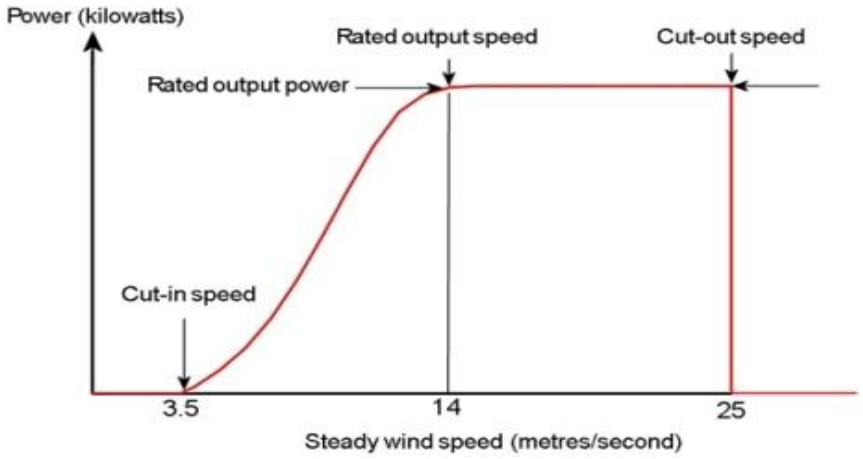

Figure 3: Typical power output vs. wind speed (WindPower Progam, 2018)

Wind turbines convert the wind's kinetic energy into rotational kinetic energy in the turbine, which in turn is converted into electricity via a generator (RAENG, 2014b). The estimation of the

available energy at a certain location is crucial to determine whether the implementation of a particular wind turbine is suitable.

The following equations from the Royal Academy of Engineering (RAENG, 2014b) are typically used to determine the theoretical maximum energy that may be harnessed from specific wind conditions:

$$P = \frac{1}{2}.\rho.A.v^3C_p \qquad [1]$$

and

$$A = \pi.r^2 \qquad [2]$$

With

v	= Wind Speed	[m/s]
P	= Power	[W]
ρ	= Density	[kg/m^3]
A	= Swept Area	[m^2]
C_p	= Power Coefficient	(according to Betz' Law)
r	= Blade Length	[m]

Figure 4 below illustrates the swept area from which a wind turbine utilises wind to generate electricity.

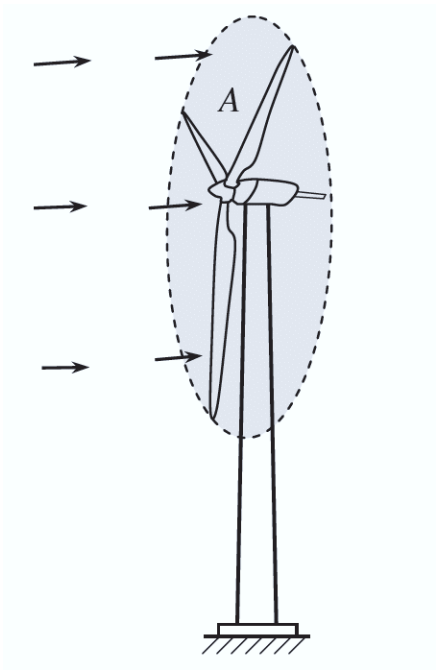

Figure 4: Swept area of a wind turbine (Tong, 2010:10)

However, according to Betz's Law, it is accepted that a wind turbine cannot be more efficient than 59.3% (Andres, 2016).

The available energy that can be extracted from the wind is approximated by (RAENG, 2014b):

$$P_{available} \approx 0.3.\rho.A.v^3 \qquad [3]$$

This equation thus aids in estimating the availability energy for certain wind speeds and rotor diameters.

The efficiency of a wind turbine is a crucial element in the design process. An efficiency of 100% would imply that the final velocity of the wind, upon leaving the swept area of the turbine, would be zero. The Betz theory assumes constant linear velocity and, in fact, the actual efficiency would be lower than the Betz Law estimation of 59.3%, since rotational forces such as wake rotation, turbulence, and tip losses would further adversely affect the efficiency of the turbine (Schubel & Crossley, 2012).

These losses may be reduced by avoiding low tip speed ratios to reduce wake rotation, or by choosing airfoils with high lift-to-drag ratios (Twele & Gasch, 2002).

2.4. Reducing the cost of manufacture

The proposed manufacturing method for the blades is rotational moulding. The blades' contribution to the total cost per turbine typically sums to approximately 10-15%, and a reduction in the manufacturing costs per blade will therefore make wind turbines for lower wind speed areas more financially feasible (Marrero *et al.*, 2014).

The conventional method of using composite materials and layering manufacture is labour intensive, with cost analysis of conventional manufacturing methods weighing labour and manufacture as more than 60% of the total commercial costs for the production of a wind turbine rotor's blades. As the blade length decreases, the percentage of costs associated with labour increases and it is therefore of paramount importance to select a manufacturing method with low labour costs and reasonable material costs to make the use of smaller wind turbines feasible (Sandia National Laboratories, 2003).

By using rotational moulding to manufacture small wind turbine blades, commercial materials may be used while also minimising labour costs. Although results are currently scarce and a quantitative analysis of the financial implications cannot be measured before commercial production of small wind turbine blades using rotational moulding has been done, experimental trails have validated the use of rotational moulding as a feasible method of manufacture to reduce production costs (Marrero *et al.*, 2014).

Rotational moulding is a method of moulding plastic with no externally applied pressure (BPF, 2018). Moulds for this technique are generally less expensive than other plastic casting processes, partly due to the pressure resistance and negation not needing to be considered for manufacture. The process entails the placement of the plastic powder in a hollow mould and, while heat is added, the mould is rotated on two axis (BPF, 2018). The polymer used in the process is then melted and takes the form of the mould it is encased in. Thereafter it is gradually cooled until the solidified shape of the desired product is attained on the inside of the mould. The product is then de-moulded and finalised with various finishing techniques (BPF, 2018).

In addition, rotational moulding is effective in producing hollow plastics with appropriate surface quality, thickness homogeneity and acceptable mechanical properties. It further gives designers some freedom in their designs and a variety of materials that may be used (Marrero *et al.*, 2014).

Consequently, rotational moulding is a viable alternative to composite material-based layering techniques that is conventionally used in wind turbine blade manufacture.

2.5. Aerodynamic design

The propulsion mechanism of wind turbines is classed as either lift- or drag induced. Generally, lift induced propulsion is more efficient than the latter, to such an extent that modern wind turbines are almost exclusively propelled by lift. Furthermore, Horizontal Axis Wind Turbines are decidedly more efficient than Vertical Axis Wind Turbines (Schubel & Crossley, 2012).

2.5.1. Betz and Glauert theories

The extensive work on wind turbines by German physicist, Albert Betz and British aerodynamicist, Hermann Glauert, simplified the basic design principles of modern wind turbine rotors (Twele & Gasch, 2002). From these theories, the blade chord length and blade twist, relative to the radius, are obtained. Moreover, the tip speed ratio, aerodynamic profile, angle of attack, and lift coefficient serve as the input parameters to these theories (Twele & Gasch, 2002).

Figure 5 shows, according to Betz's theory, a rough estimation of the power production of a wind turbine based on the wind speed and rotor diameter.

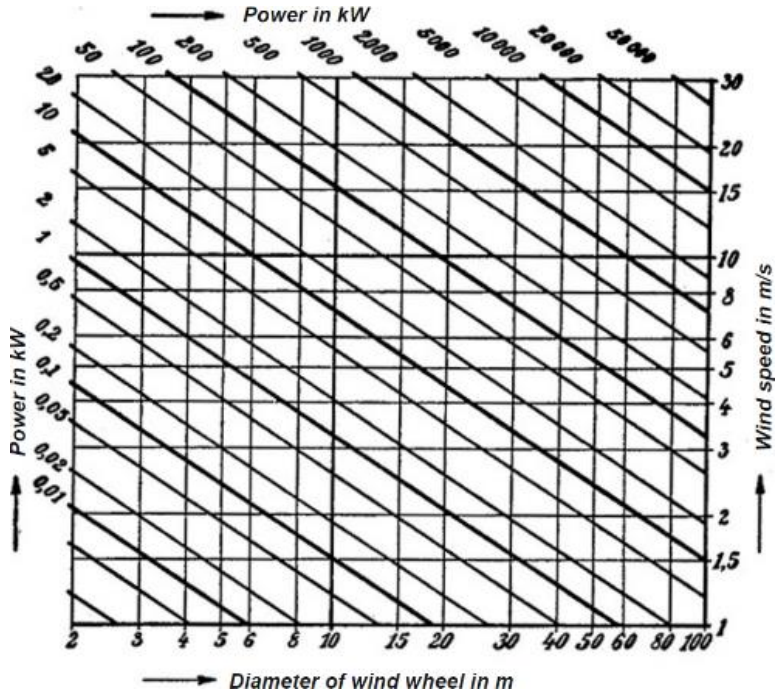

Figure 5: Power of wind turbines according to Betz's theory (Gasch *et al.*, 2012:172)

While Betz's theory may be used to estimate and predict wind turbine performance, Glauert's work includes the refinement of Max Munks's thin airfoil theory. The thin airfoil theory connects angle of attack to lift, conceptualising the airflow over an airfoil with a thickness of zero and infinite length, as two dimensional (Twele & Gasch, 2002).

Elaborating on the thin airfoil theory, wind turbine blades may be considered as airfoils with the same aerodynamic principles applied to their functioning, respecting lift, drag and dimensioning.

2.5.2. Basic airfoil theory

To evaluate the capability of a specific turbine blade to harness energy from wind, the blade and airfoil geometry is used to determine the lift and drag generated with certain conditions. Lift and drag of an airfoil is dependent on a number of factors, as illustrated in Figure 6, which shows the parameters that dictates the drag (D) and lift (L) of an airfoil.

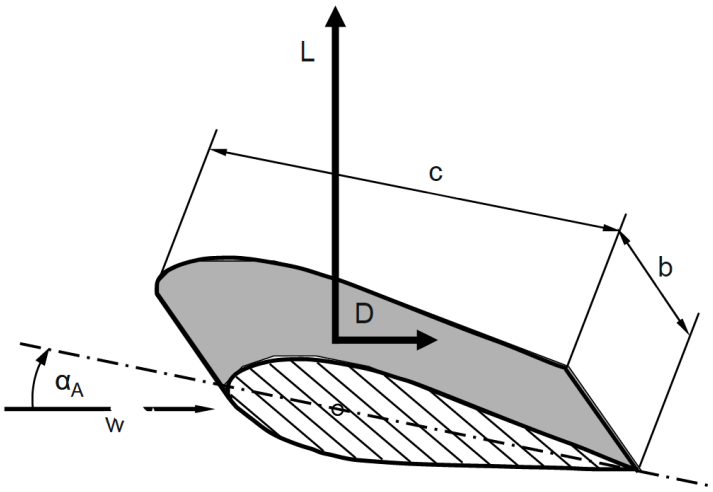

Figure 6: Lift and drag forces of an airfoil (Gasch *et al.*, 2012:175)

The lift and drag coefficients are experimentally determined for various airfoils and the resulting force on the airfoil can then be determined by using (Gasch *et al.*, 2012):

$$F_{res} = \sqrt{L^2 + D^2} \qquad [4]$$

As long as the airflow is aerodynamically attached to the airfoil, the force acts on a point of approximately 25-30% of the chord length. To illustrate the forces acting on an airfoil when exposed to wind, the Figure 7 shows the forces at the applicable angle of attack (α_A).

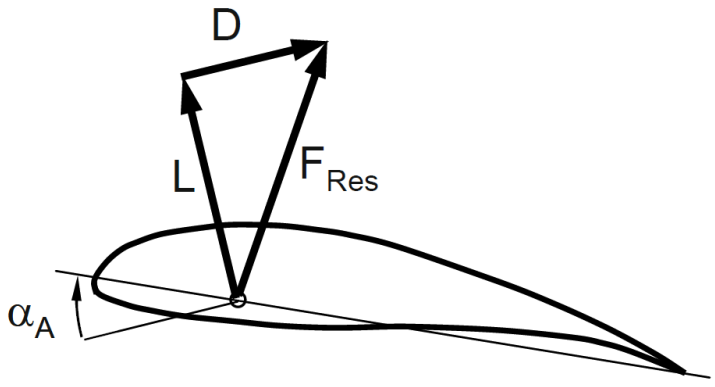

Figure 7: Drag, lift and resulting force on airfoil (Gasch *et al.*, 2012:178)

It is evident that the lift and drag forces are heavily dependent on the angle of attack on the airfoil and must therefore be carefully considered during the design process.

2.5.3. Blade planform geometry

The performance of a wind turbine is largely subject to the design of the rotor blades. The geometry of the turbine blades must therefore be taken into consideration in order to optimise the wind turbine for the desired wind specifications (DNV, 2002). A typical wind turbine blade profile is illustrated in Figure 8.

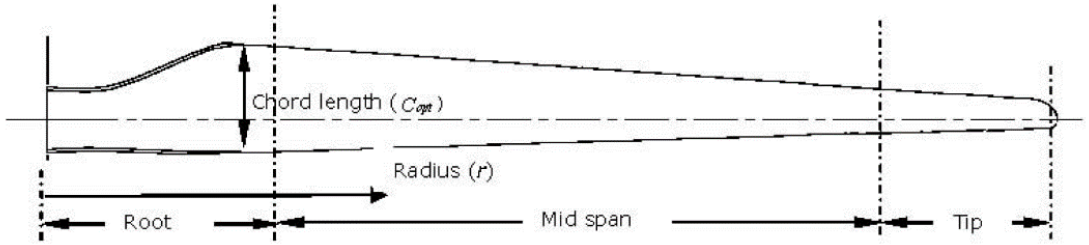

Figure 8: Wind turbine blade profile (DiFrangia, 2014)

An important factor that dictates the ideal blade geometry of a wind turbine is the tip speed ratio, which is defined as the relationship between the relative wind velocity and the tip of the rotor blade's velocity (REUK, 2018).

Tip speed affects the efficiency, torque, noise generation, mechanical stress and aerodynamic qualities of the turbine rotor. Consequently, higher tip speeds must be accompanied by narrower blade profiles (REUK, 2018). However, a narrow blade profile is more susceptible to failure due to the increase in relative stress generated by centrifugal and aerodynamic forces (Schubel & Crossley, 2012). Care must therefore be taken to ensure that narrowing the blade profile does not decrease the structural integrity of the blade in such a way that it will fail under expected wind conditions.

The ideal chord length for a blade profile can be determined by considering various theories and methods. These theories provide the basic shape and advanced methods are then used to optimise the blade geometry (Hau, 2013).

The completed optimised blade planform geometry is difficult to calculate with analytical methods, but complex numerical methods may be used for blade optimisation to increase its efficiency (Chatott, 2003; Fuglsang & Madsen, 1999; Jureczko *et al.*, 2005).

The approximations and calculations discussed above serve as basic input to the design process and may be refined using FEM (Finite Element Method) and CFD (Computational Flow Dynamics) software (Tenguria *et al.*, 2010).

2.5.4. Blade element and blade element momentum theories

To design a wind turbine rotor, the wind turbine theory of William Froude, David Taylor and Stefan Drzewiecki proves a valuable tool (Shih-Yu *et al.*, 2013). This method is based on the principle of dividing the rotor blade into sections and then determining the forces and effects on each segment. The various forces of each segment are then aggregated to determine the characteristics for the full length of the blade (Ingram, 2011).

However, this method only considers the model as two-dimensional and neglects the chord thickness. For every segment of the blade, a force balance is applied regarding the thrust and torque generated by the drag and lift of the airfoil, while axial and angular momentum is balanced simultaneously. This yields non-linear equations that must be solved iteratively to find the characteristics and performance of the rotor.

The following figure shows how the blade may be divided.

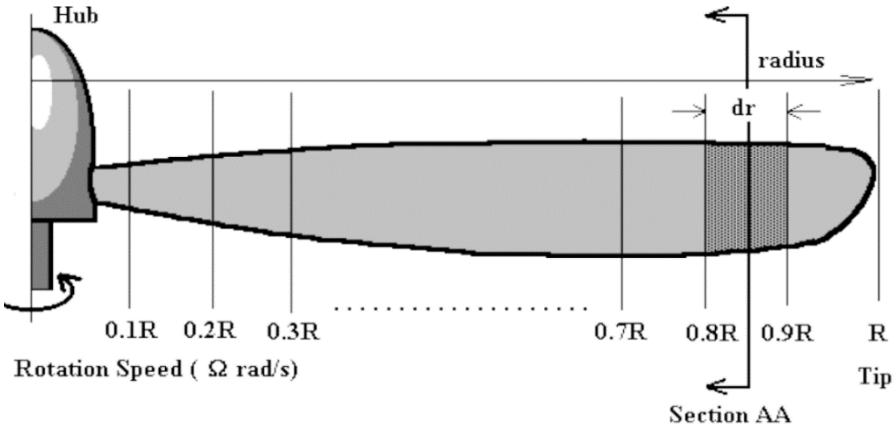

Figure 9: Segmenting a rotor blade for BEM (Auld & Srinivas, 2017)

Secondary effects related to 3D flow velocities fall outside the scope of this method, disregarding shed tip vortex and radial components associated with a three-dimensional model. This theory will therefore over-predict the thrust delivered and under-predict the produced torque (Auld & Srinivas, 2017).

Even though this theory has shortcomings, it is an effective method to introduce the optimisation of a wind turbine rotor (Auld & Srinivas, 2017).

The blade element theory's principles provide the basis for the Blade Momentum Theory (Gasch *et al.*, 2012).

Figure 10 below illustrates the velocities and angles considered in the blade element theory that is utilised in the performance analysis of the blade.

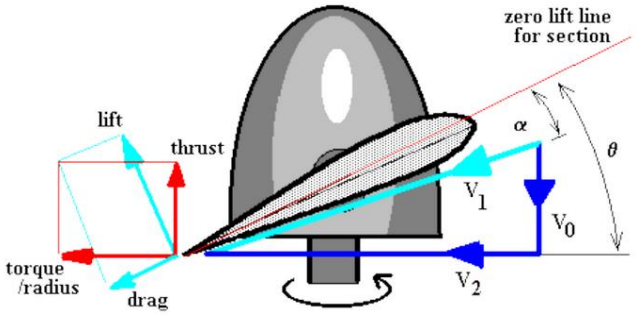

Figure 10: Velocity factors and directions of forces of airfoil profile (Auld & Srinivas, 2017)

Where

V_0 = Axial flow velocity
V_1 = Section's local flow velocity
V_2 = Angular flow velocity
θ = Pitch angle
α = Angle of attack
φ = Pitch angle (θ) – Angle of Attack (α)

Furthermore, the torque (Q) and thrust (T) per section of the rotor is determined by using the following equations (Gasch *et al.*, 2012):

$$\Delta Q = \frac{1}{2} B.c.r.\frac{V_\infty(1-a)}{sin(\varphi)}.\frac{\Omega.r.(1-b)}{cos(\varphi)}(C_L.\sin(\varphi) - C_D.\cos(\varphi)).dr \quad [5]$$

and

$$\Delta T = \frac{1}{2} B.c.\frac{{V_\infty}^2(1-a)^2}{sin^2(\varphi)}(C_L.\cos(\varphi) + C_D.\sin(\varphi)).dr \quad [6]$$

With

ρ = Air Density
c = Blade Section Chord Length
C_D = Section Drag Coefficient
C_L = Section lift Coefficient
B = Number of Rotor Blades
r = Radius at Section Position
dr = Section Width

These equations are the first step in the theory's iterative process to determine the thrust and torque of the rotor.

To find values for corrected wind speeds (as defined by V_0, V_1 and V_2), the inflow factors must be determined (Auld & Srinivas, 2017).

The calculation of V_0 and V_2 is complicated by the induced flow effect of the wind passing through the turbine. While V_0 is roughly equal to the location air speed and V_2 equal to the sectional angular speed – dependent on the rotor's rotational speed – these components are altered by the induced flow around the rotor. The inflow factors are designated "***a***" as the axial inflow factor, and as "***b***" for the swirl factor related to angular inflow and must be determined by numerical iterative methods from a combination of the following equations (Auld & Srinivas, 2017).

The accurate values for V_0, V_1 and V_2 can be quantified as (Auld & Srinivas, 2017):

$$V_0 = V_\infty - a.V_\infty \qquad [7]$$

and

$$V_1 = \sqrt{V_0^2 + V_2^2} \qquad [8]$$

and also

$$V_2 = \Omega.\,\mathrm{r} + \mathrm{b}.\,\Omega.\,\mathrm{r} \qquad [9]$$

With

V_∞ = location air speed
Ω = rotor's rotational speed

The angle of attack (α) is calculated with the following equation (Auld & Srinivas, 2017):

$$\alpha = \theta - \tan^{-1}\left(\frac{\mathrm{V_0}}{\mathrm{V_2}}\right) \qquad [10]$$

To determine the values for the still unknown inflow factors ***a*** and ***b***, the principle of momentum conservation is combined with the blade element theory as follows (Gasch *et al.*, 2012):

Based on Bernoulli's equations for flow and the conservation of momentum and by balancing pressure and area with thrust delivered, the rotor's thrust is given by the following equations (Gasch *et al.*, 2012):

$$\Delta\mathrm{T} = \rho.\,4.\,\pi.\,\mathrm{r}.\,\mathrm{V}_\infty^2(1-\mathrm{a})\,\mathrm{a}.\,\mathrm{dr} \qquad [11]$$

The torque of the rotor is, according to the same principles as above, defined as

$$\Delta\mathrm{Q} = \rho.\,4.\,\pi.\,\mathrm{r}^3.V_\infty(1-\mathrm{a})\,\mathrm{b}.\,\Omega.\,\mathrm{dr} \qquad [12]$$

The values for the inflow factors ***a*** and ***b*** may now be determined by iteration from the four equations related to torque and thrust and, also, the equations for the axial and radial velocity factors. The values for torque and thrust from the blade element theory and the momentum theory must converge and the converged solution's corresponding values for **a** and **b** will then be used in the accurate prediction of the turbine's performance.

Consequently, the convergence of the iterative process results in the prediction of torque, thrust, correct velocity factors and, therefore, also the power delivered by the turbine.

2.5.5. Ideal chord length

In order to design efficient wind turbine rotors, the chord length must be determined and applied to the model. For each part of the rotor's sectioned blade, the ideal chord length is determined from the following equations (Ingram, 2011):

$$C = \frac{8.\pi.r.\cos\beta}{3.B.\lambda_r} \qquad [13]$$

and

$$\beta = 90° - \frac{2}{3} tan^{-1}(\frac{1}{\lambda_r}) \qquad [14]$$

Where

C = Ideal Chord Length
r = Section Radius
B = Number of Blades
λr = Section Tip Speed

Tip speed is defined as (Schubel & Crossley, 2012):

$$\lambda = \frac{\Omega.r}{V_w} \qquad [15]$$

With

Ω = Rotational Velocity
R = Rotor Radius
V_w = Wind Velocity

Considering these equations, it is possible to calculate the ideal chord length for a wind turbine's blade sections.

2.6. Structural blade design

In this section, the structural design aspects of wind turbine designs are reviewed. Due to the forces acting on a wind turbine during operation, it is important that the blades are designed to have sufficient structural properties to convert the wind into torque, without any risk of structural failure. The structural design process aims to ensure that the wind turbine rotor can extract power from wind, without failure of the blades.

2.6.1. Classifying loads acting on a wind turbine

The operational environment and subsequent operation of a wind turbine causes various forces to be exerted on the blades. In this study, certain limitations and assumptions are made regarding the loads applied in the design process, but a thorough review of relevant forces is included.

While there are many approaches to classifying the types of loading on the rotor, a simple method to segregate these forces is as follows. Loads applied to the rotor may be classified as either steady, cyclic, transient, stochastic, or resonance induced (Manwell & McGowan, 2009). Each of these loads is explained below (Manwell & McGowan, 2009:158-160):

Steady loads can be static or rotating and does not generally vary much over time. Static steady loads are the non-time varying loads applied to a non-moving structure, such as wind blowing at a steady speed against the wind turbine tower. Rotating steady loads include the forces acting on the blades resulting from steady rotor rotation during operation.

Cyclic loads refer to regularly varying loads, such as the loads particular to the rotation of the rotor. Due to the weight of the rotor blades and wind shear acting on these blades, the load on different parts of the structure fluctuate as the rotor turns.

Transient loads vary with time and occur due to an external event acting on the turbine. While oscillations may occur for this type of disturbance in the system, they generally decay as time passes. An example of a transient load is the effect the brake has on the turbine system when it is suddenly applied and released.

Stochastic loads vary with time and in a generally unpredictable manner. A possible cause of this type of load may be severe and sudden wind turbulence.

Resonance-Induced loads are caused by some form of vibration in the system at a natural frequency of one or more part and the wind turbine's response to this disturbance in a dynamic manner. This occurs due to unforeseen circumstances during operation, or simply due to negligent design that does not account for the impact of vibration on the system.

The aforementioned loads are caused by either mechanical control of the system, gravity, dynamic interactions between the system and environment, or aerodynamics (Manwell & McGowan, 2009). Successfully identifying the source of the loads that may act on the system and then addressing each of these sources sensibly during the design phase, will simplify the maintenance and operation of a wind turbine.

2.6.2. Specific blade loading

Structurally, each blade may be divided into three sections and each can be considered separately. First, the *blade root* carries the highest loading of the blade, while the low relative wind velocity at this section leads to low lift. It is therefore important to ensure that this section is structurally sound to handle the structural demands resulting from gravity and the wind acting on the blade. Second, the *mid span*'s role is more aerodynamic than structural, and the lift-to-drag

ratio should be maximised in this area. The slimmest airfoil profile should be applied to this area, as long as the structural integrity is not compromised. Finally, the *tip* is critical, from an aerodynamic standpoint, to the performance of the turbine blade. In this section, the lift-to-drag ratio must also be maximised. Using specialised designs for this section can reduce noise pollution and improve the effectivity of the rotor by reducing, associated losses (Schubel & Crossley, 2012).

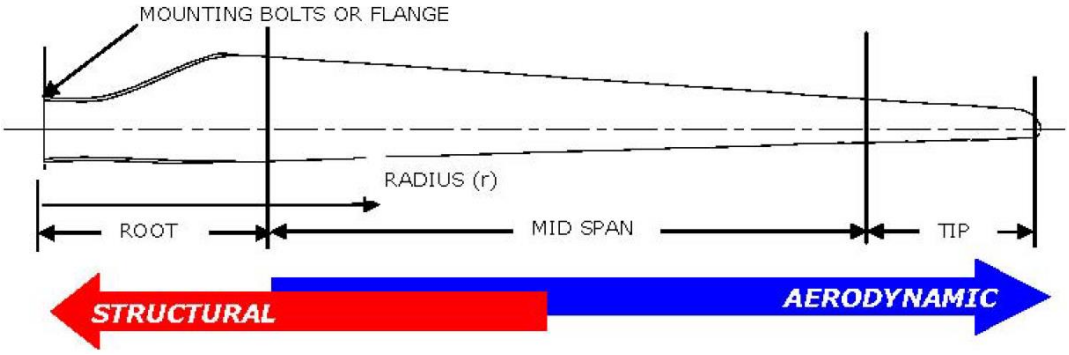

Figure 11: Regions of blade loading (Schubel & Crossley, 2012:3446)

The forces applied to a wind turbine during operation is generally classified as either 'edgewise' or 'flapwise' (Tong, 2010) and is illustrated in Figure 12. Generally, flapwise structural reinforcement is needed to ensure that the blade is strong enough to cope with the aerodynamic forces acting on it, while edgewise strength is needed to protect the blade from failing due to its own weight.

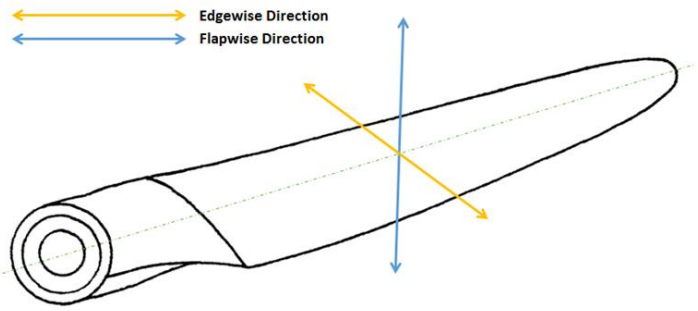

Figure 12: Flapwise and edgewise loading (National Instruments, 2016)

2.6.3. Finite element analysis

Due to the varied nature of the loads that result from wind, computer-based finite element models are widely used to do structural analysis on wind turbine rotors. Finite element method (FEM) analysis is useful in investigating behaviour that includes global stress/strain levels, tip deflection,

and Eigen frequencies (Tarfaoui & Shah, 2013). The global behaviour can be determined by using a simple shell model, while more complicated 3D models are used to determine localised behaviour. Therefore, the design of modern wind turbine blades is made simpler with the use of modern computer-based structural analysis tools (Tenguria *et al.*, 2010).

2.6.4. Centrifugal force overview

Consideration of the centrifugal forces acting on the blades depend on the weight and rotational speed of the turbine and the stress can be determined by considering Figure 13:

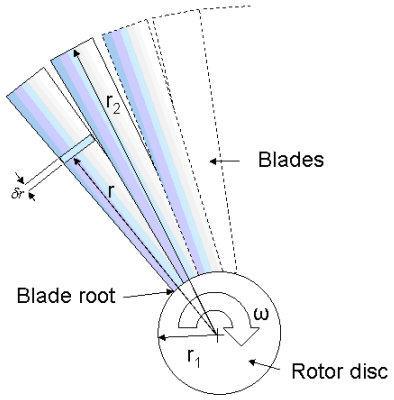

Figure 13: Simplified blade dimensions (RAENG, 2014a:2)

The equations for the centrifugal force are shown below (RAENG, 2014a):

$$F = \rho . A . \omega^2 \frac{(r_2{}^2 - r_1{}^2)}{2} \qquad [16]$$

and

$$\omega = \frac{\text{rpm} \times 2\pi}{60} \qquad [17]$$

With

F	= Resulting Centrifugal Force	[N]
ρ	= Density of Material	[kg/m^3]
ω	= Rotational Speed	[rad/s]
r_2	= Upper bound Radius	[m]
r_1	= Lower Bound Radius	[m]
rpm	= Rotations per Minute of Rotor	

The stress exerted on the material can now be defined by (RAENG, 2014a):

$$\sigma = \frac{F}{A_{root}} \qquad [18]$$

σ	= Stress on material
F	= Centrifugal Force
A_{root}	= Area at Blade Section

With these equations, the centrifugal stresses induced can be determined. It is evident that the rotational speed, density of the material, and length of the blade are all to be taken into consideration, with respect to the stress on the blades.

2.6.5. Shear stress overview

The shear formula is used to determine the stress the material undergoes due to force exerted on it (Hibbeler, 2013). The shear force is zero at the outermost point of the section – furthest away from the neutral axis – and maximum at the neutral axis. The shear formula is formulated as follows (Hibbeler, 2013):

$$\tau = \frac{V.Q}{I.t} \qquad [19]$$

With

τ	= Shear stress at distance *y* from neutral axis	[Pa]
V	= Shear force, as previously defined	[N]
Q	= Statical moment of Section	[m^3]
I	= Moment of Inertia	[kg/m^3]
t	= Cross Sectional Width	[m]

The shear stress is distributed in the following way:

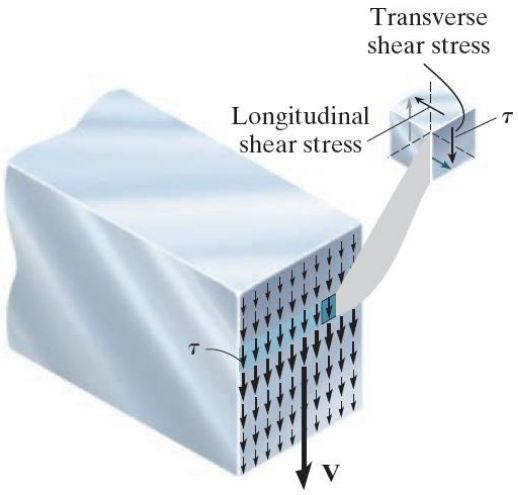

Figure 14: Shear stress distribution (Hibbeler, 2013)

Regarding shear stress, the distribution of the rotor shape around the neutral axis and the thickness of the airfoil's shell is of importance.

2.6.6. Normal stress overview

The normal stress acting on the blade's sections is a function of the resultant internal momentum (Hibbeler, 2013) and is defined as follows:

$$\sigma_{max} = \frac{M.c}{I} \qquad [20]$$

With

σ_{max}	= Maximum normal stress in the member	[Pa]
M	= Shear force, as previously defined	[N.m.]
c	= Distance from the neutral axis to farthest point on section	[m]
I	= Moment of Inertia	[kg/m^3]

In contrast with the shear stress of a section, the normal stress is the highest at the points furthest away from the neutral axis, and zero on the neutral axis itself (See Figure 15).

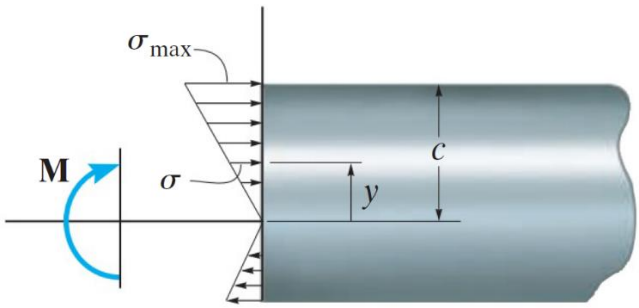

Figure 15: Normal stress distribution (Hibbeler, 2013)

It is evident from the above figure that it acts perpendicularly to the direction of the applied force.

2.6.7. Combined stress analysis

Due to the multi-dimensional nature of the forces exerted on the rotor, the stress analysis is conducted as a combination of the normal, shear and centrifugal components. The centrifugal force's induced stress will contribute to the total normal stress at the blade's outer edge, as well as contributing to the maximum in-plane stress, as an additional component to the shear stress induced. The specific nature of this analysis is explained in greater detail in future chapters.

2.7. Optimisation of rated wind speed for maximum power output

In order to maximise the annual energy production (AEP) of a specific rotor, the ideal design wind speed (rated wind speed) must be determined. This is done by using wind data from a specific area or region in which the turbine is to be installed. Optimising the AEP by adjusting the design wind speed of the rotor is a particularly suitable method for low wind speed areas, because the

aerodynamic design of wind turbine blades is already highly optimised. Adjusting the design wind speed can therefore enhance the AEP's optimisation.

To calculate the optimised wind speed, statistical analysis of the area's wind data was conducted in order to determine what wind speed will deliver the maximum power output over the course of a year. A Weibull distribution function is particularly valuable to analyse the wind distribution per annum and also to find functions that will model the peak annual energy production (Sedaghat *et al.*, 2017).

In order to complete the Weibull distribution analysis, the following Weibull parameters are used (Sedaghat *et al.*, 2017):

$$f(V) = (\frac{\mathrm{k}}{\mathrm{c}})(\frac{\mathrm{V}}{\mathrm{c}})^{\mathrm{k}-1}\exp\left[-\left(\frac{\mathrm{V}}{\mathrm{c}}\right)^{\mathrm{k}}\right] \qquad [21]$$

Consider *k* the shape factor, *c* the scale factor, and *V* the wind speed. The scale factor *c* can be determined by using the following gamma function (Sedaghat *et al.*, 2017):

$$c = \frac{V_{mean}}{\Gamma(1+\frac{1}{k})} \qquad [22]$$

where V_{mean} is the average wind speed per year, and *k* the shape factor.

The shape and scale factors are determined by matching the Weibull distribution function to the dataset obtained for an area and is then used in the determination of the Capacity Value (C_v) that is directly used in the optimisation of the AEP.

The Capacity Value is determined as (Sedaghat *et al.*, 2017):

$$\mathrm{C_V} = \int_{cut-in}^{ratedspeed} \mathrm{V}^3 f(V)\,\mathrm{dV} + \mathrm{V}_{\mathrm{rate}}^3 \int_{ratedspeed}^{cut-out} f(V)\,\mathrm{dV} \qquad [23]$$

With *f(V)* as defined above and *cut-in/cut-out* defined as the cut-in and cut-out wind speeds. V_{rate} is the value to be determined from the above methods and functions. The dimensionless capacity value represents the annual power production. It is not based on the size of the rotor and is derived solely from the unknown V_{rate}. An optimised rated speed can therefore be obtained by simply maximising the function of C_v with regards to the rated speed (Sedaghat *et al.*, 2017).

2.8. Gust-wind conditions

Gust-winds are brief and rapid increases in the speed of wind, and typically last for less than 20 seconds, after which the wind speeds regress to normal conditions.

In order for a wind turbine's rotor to operate safely, it should be able to withstand these gust-wind conditions. Even though these conditions only last for seconds at a time, it can cause considerable damage if not considered during the design phase.

The following illustrates how the approximate maximum gust-wind speed for the chosen location is calculated (Cvitan, 2003):

$$V_g = k_g . V_{mean} \quad [24]$$

Where

V_g = Maximum Gust Speed [m/s]
k_g = Gust Factor
V_{mean} = Mean Measured Wind Speed [m/s]

With

$$k_g = 1 + \frac{2.28}{\ln(\frac{z}{z_0})} \quad [25]$$

With

z = Height Above Ground [m]
z_0 = Roughness Length [m]

The determination of gust-wind conditions provides the parameters by which modern wind turbines are designed and it is therefore integral in determining whether the rotor can operate safely in a specific region.

2.9. Summary

The literature has shown that, in order to successfully develop a wind turbine rotor for low wind speed conditions, conventional rotor design procedures are utilised and adapted in order to make provision for low wind speeds and cost efficiency. The integration of aerodynamic and structural design methods into a single working model can be done as outlined in this chapter and the design input can be determined by optimising the statistical data used for rated wind speed. The following chapters provide the detailed design methods that may result in a working model.

CHAPTER 3 AERODYNAMIC DESIGN PREMISE

In order to design the rotor blade, the geometry, angle of pitch, and length of the blade is integrated in a manner that will produce the maximum power output per year. In this study, the structural integrity of the blade serves as the limiting factor in the size of the rotor. The rotor will have a basic shell structure and containing no internal support or reinforcement and is developed with a pre-determined material.

The model used in the design of the blades is composed in such a way that the aerodynamic and structural design is integrated. This is done to ensure that the structural properties of the blade and of its materials will limit the length of the blade, while the aerodynamic design determines the shape of the blade. The aerodynamically determined blade shape is scaled to the structural design's specifications, to ensure it will not fail during operation.

Therefore, the first step in the design process is the aerodynamic design, entailing the blade pitch angles, preliminary length of the blade, chord length, and forces (thrust and torque) that will be exerted on the rotor, due to the power of the wind and rotational energy.

3.1. Optimising wind speed for local conditions

In order to maximise the annual power output of the rotor, the design is based on the optimisation of the blades to suit local wind conditions (Potchefstroom, North-West). The literature review provided the background for this method (Section 2.7). The first factor to consider is the range of wind speeds that the rotor is designed for, since it determines the power output characteristics and also the forces on the blade. The optimal wind speed that will result in a maximum power output per year is determined by using a Weibull distribution and real-wind data for the area. By using the *k* and *c* values from the Weibull distribution, the optimal wind speed is calculated and applied during the design of the rotor.

3.1.1. Optimisation regarding local wind speed data

In order to determine the necessary *k* and *c* values, a Weibull distribution is matched to the recorded wind data obtained for the Potchefstroom area (SAWS, 2016). This is done by first sorting the data into various statistical bins, based on Rice's rule for selecting the number of bins.

Rice's rule is defined as $\mathbf{J = 2n^{1/3}}$, with *J* the number of bins, and *n* the number of measurements. However, the application of this rule was simplified to ease the processing of the data. This was done by means of rounding and standardising the recommended step size for the bins to a

mathematically feasible number, thus making the step size of the bins more practical at step sizes of 0.25 m/s.

The optimisation was done by matching the power in the wind-per-area graph, defined as $\mathbf{P = 0.5\ \rho\ V^3}$ (with *P* the power, *ρ* the air density, and *V* the wind speed), to a Weibull distribution from the data. The matched values for *k* and *c* were then used in the maximisation of C_v (or Capacity Value), as discussed in Section 2.7.

Some of the results regarding the Weibull distribution analysis are displayed in the Table 1.

Table 1: Wind data statistical overview

Year	Number of Data Points	Data Loss due to Wind Station Recording Failures [%]	Calculated Number of Bins	Simplified Number of Bins	Average Wind Speed [m/s]	Maximum Recorded Wind Speed [m/s]	Average power in the Wind [W/m^2]
2011	8376	4.38	40.62	46	2.11	11.1	16.37
2012	8712	0.55	41.15	46	2.32	9.6	20.2
2013	8446	3.58	40.72	46	2.27	10.2	18.28
2014	8467	3.34	40.76	46	2.21	9.9	16.1
2015	8662	1.12	41.07	46	2.32	10	19.37
2016	8592	1.92	40.96	46	2.36	9.8	20.77

Due to the loss of data, because of recording equipment malfunctions, and the seasonal nature of wind speeds in the area, the data of 2013 and 2014 could not be matched to a Weibull distribution and was therefore not used in the optimisation process. However, the nature of the data from these two years match the collective data from other years (such as average wind speed and maximum recorded speeds) in such a way that it could be disregarded, without compromising the integrity of the optimisation process.

Per annum, matching the dataset to the Weibull distribution by means of Microsoft Excel's Solver, the values for *k* and *c* were determined. Substituting these values into the equation for C_v and then optimising for a maximum C_v value gave the following results:

Table 2: Results of matching Weibull distribution to dataset

Year	k - value	c - value	Capacity Value	Optimised Rated Wind Speed [m/s]
2011	28.65	2.15	284.52	1.99
2012	30.04	2.37	253.10	2.19
2015	31.13	2.37	146.4	2.19
2016	32.83	2.40	115.4	2.23

The optimal rated speed to be used in the design for the low wind speed area of Potchefstroom is taken as the average of the annual recommended wind speeds, which is **2.15 m/s**.

3.1.2. Verification of the method

To verify the correctness of the application of this method to Potchefstroom's data, the same method was applied to data obtained from areas in Kuwait and its stated results. This study was conducted by Sedaghat *et al.* (2017) and presented in their article *Determination of rated wind speed for maximum annual energy production of variable speed wind turbines*.

Comparing the study's results with those of Sedaghat *et al.* (2017), the following results comparison can be made:

Table 3: Verification of optimisation method

Location	Rated Wind Speed [m/s] (Sedaghat et al. (2017))	Rated Wind Speed [m/s] (Calculated with Method)
Al Wafra	17	17.46
Al Taweel	17	17.01
Umm Omara	17	16.14
Ras As-Subiyah	16	15.54
KISR	15	14.81
Rawdatain	15	15.00

From the above comparison, it may be concluded that the method was applied accurately in determining the optimal wind speed for an aerodynamic design of the wind turbine's blade that would optimally function in the Potchefstroom region. The discrepancies may be attributed to the fact that Sedaghat *et al.* (2017) interpreted charts to obtain values, while the method used in this study was based on a numerical solution that was calculated using MS Excel's built-in Solver function.

The application of this optimisation method is therefore accepted to be accurate when used with the data from the South African Weather Service (SAWS, 2016) and the rated wind speed of 2.15 m/s was assumed to be the correct optimum wind speed on which to base the aerodynamic design.

3.1.3. Determining gust-wind speed

To determine the speed of expected gust wind conditions and, therefore, the maximum wind speed the wind turbine rotor must be able to withstand, the methodology is used as discussed in Section 2.8.

From local wind speed data (SAWS, 2016), the maximum mean-measured wind speed (V_{mean}), during the period of 2011 to 2016, was 11 [m/s]. The roughness length (z_0) (Mabille, 2014) for the selected area, Potchefstroom, is 0.1 and the height above ground (z) is taken as 5 [m].

By using these values in the above equations, the maximum gust-wind speed is calculated as **17.5 [m/s]**. This serves as the speed at which the rotor blades is designed to be structurally safe.

3.1.4. Wind data analysis and conclusion

Table 4 displays an overview of the distribution of wind speed in the Potchefstroom area as, provided by SAWS (2016), expressed as a percentage of each year.

Table 4: Wind speed time distribution for Potchefstroom are per annum

Wind Speeds [m/s]	2011	2012	2013	2014	2015	2016	Average for 2011-2016
0-2	41.19%	36.69%	37.45%	37.40%	35.28%	36.51%	36.42%
2-4	45.93%	46.24%	46.50%	48.81%	48.67%	45.20%	46.89%
4-6	10.66%	13.43%	13.41%	12.09%	13.02%	14.98%	12.93%
6-8	1.85%	3.47%	2.57%	1.52%	2.72%	3.10%	2.54%
8-10	0.33%	0.18%	0.06%	0.15%	0.29%	0.20%	0.20%
10-11.25	0.05%	0.00%	0.01%	0.01%	0.01%	0.01%	0.02%

From the above table it is evident that – measured over a six-year period – the average wind speed is very low during most of the year, exceeding on average 6 m/s for less than three percent of the year.

Therefore, the ***optimal design speed*** for the turbine is calculated to be **2.15 m/s** and is used during the aerodynamic design to fix the geometry of the rotor blade. After fixing the geometry and profile of the blade, the ***maximum wind speed*** is used to evaluate the degree to which the blade may be scaled, while still able to structurally withstand a gust-wind of **17.5 m/s**, thus effectively determining the maximum length of the blade.

3.2. Airfoil characteristics and profile

The design for the rotor blade was based on a predefined airfoil profile, designated by the code *AE02-160ST* (Bosman, 2003). The following image shows a visual representation of the original profile; the profile pitched to a certain degree and, lastly, scaled when shorter chord length is desired.

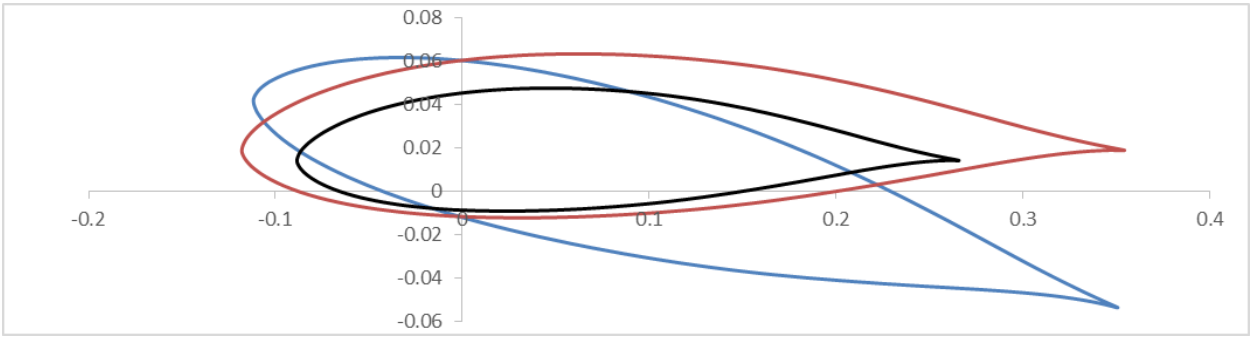

Figure 16: Original airfoil profile (Red), shorter chord length (Black), pitched profile (Blue) (Bosman, 2003)

This profile formed the basis of the aerodynamic design, being scaled and pitched in order to maximise the power extraction from the wind.

In order to model and predict the behaviour of a rotor, MS Excel was used to calculate the influence of the wind on torque and thrust delivered. In order to achieve this, the blade was divided into sections (see Section 3.3), each with its own chord length and specifications, and each section was aerodynamically and structurally evaluated. By tallying the effect of the wind on each section, an accurate representation of the blade's performance was determined.

An integral part of the aerodynamic design of the blades was the lift and drag coefficients, associated with various pitch angles and Reynolds' numbers. This was determined in the form of datasets from the software package XFOIL (MIT, 2007), and an example of such a dataset is shown in Table 5. Different Reynolds' numbers resulted in different values for lift and drag (C_L and C_D) for the same angles of attack (MIT, 2007).

Table 5: Lift and drag coefficients for a Reynolds' number of 200000 and 650000

Angle of Attack [degrees]	CL_{200000}	CD_{200000}	CL_{650000}	CD_{650000}
-2	-0.015	0.01517	-0.0013	0.00703
-1	0.0881	0.0155	0.1146	0.00693
0	0.1919	0.01561	0.2305	0.00693
1	0.2966	0.01544	0.3459	0.00697
2	0.3965	0.01521	0.4604	0.00706
3	0.4977	0.01472	0.5735	0.00728
4	0.5960	0.01419	0.6833	0.00768
5	0.6991	0.01369	0.7891	0.00833
6	0.8296	0.01358	0.8869	0.00943
7	0.9743	0.01429	0.9758	0.01100
8	1.0097	0.01553	1.0497	0.01318
9	1.0594	0.01840	1.0962	0.01607
10	1.0807	0.02445	1.1452	0.01943

To determine the correct lift and drag for Reynolds' numbers, between those generated by XFOIL, simple interpolation was assumed to be sufficiently accurate.

3.3. Sectioning the blade

In order to design the blade accurately, the blade was sectioned into evenly spaced geometric sections, spaced from root to blade tip. While more sections would undoubtedly result in more accurate predictions of the blade's aerodynamic and structural performance, ten sections were chosen, since a higher number of sections would prolong the calculations and modelling. Due to the iterative process of design and the unknown final length of the blade, opting for additional sections would exceed the scope of sizing a wind turbine rotor and also negate the practicality of using an integrated and largely analytical model. Section 2.5.4 provides an example of a sectioned blade, designated in terms of the total length of the blade with radius *R*.

3.4. Ideal chord length

While the profile of the blade is fixed, the scale or size of the airfoil's profile is adapted to fit the conditions the rotor is subjected to in order to maximise the power output of the turbine (see Section 3.2). This is done by determining the ideal chord length and then scaling the profile to fit the calculated chord length (Ingram, 2011).

The ideal chord length is determined (as per the methods discussed in Section 2.5.5) in such a manner that the results may be considered functions of the rotor blade length and wind characteristics for the specified area, Potchefstroom. This was conducted as part of the integrated design and the ideal chord length was calculated as part of the iterative design process. The MS Excel for the iterative design can be found in Appendix A (see Table 24). The results for this method are illustrated, in the discussion in Chapter 5, of the iterative design process's results.

3.5. Blade element momentum (BEM) theory

In order to analyse the blade's performance, the blade element momentum theory is used, by which a force balance is applied at each section of the blade. It further includes the lift and drag for each section, so as to provide the performance characteristics of the blade in terms of torque and thrust, which allows for the generated power to be determined from the rotor RPM and torque delivered. This theory disregards secondary effects associated with three-dimensional flow velocities, such as those induced by tip vortexes or the flow induced by the rotor's rotation. It also over-predicts the power delivered by the rotor.

The full implementation of the theory, as discussed in Section 2.5.4, is illustrated in Appendix A. The built-in MS Excel Solver is used to determine the numerical solution to the inflow factors **a**

and **b**. The converged solutions for the inflow factors also provide the solution to the rotor characteristics, which can be found in Appendix B.

3.6. Summary

The aerodynamic design of the rotor blades will serve as the input for the structural design. The goal of the structural design is, therefore, to ensure that the blades can produce maximum power per year without failing due to the forces exerted on it, which is determined by the aerodynamic design.

The following chapter explores how the structural design and aerodynamic model is integrated to maximise the rotor blades into a single model.

CHAPTER 4 STRUCTURAL DESIGN PREMISE

By applying the BEM Theory with the design wind speeds, as determined by the optimisation of Potchefstroom's wind data, an MS Excel model was developed to effectively determine the maximum size of the rotor blades.

As the power output of a rotor is directly related to the rotor diameter, the final model was developed to in such a way that the integrated design calculations were mostly written as functions of the blade length and, thus, enabling the maximisation of annual power output by considering blade length as a primary consideration factor.

The integrated design considers the following as input:

Aerodynamic (to determine blade shape)

- Design Wind Speed
- Air Density
- Dynamic Viscosity of Air
- Rotor design RPM
- Number of Blades

Structural (to determine blade length)

- Material Modulus of Elasticity
- Material Yield Strength
- Material Density
- Airfoil Skin Thickness

The model's output will be (final design specifications)

- Maximum Blade Length as dictated by resultant Safety Factors for the material
- Pitch Angle per Section
- Chord Length per Section
- Turbine Power Output per Year

It is important to note that the model is written in its entirety as functions of the mentioned variables, in order to determine the ideal blade length. Therefore, the model is able to recalculate automatically if any of the input is changed. As a consequence, the blade length is increased only until it satisfies the safety factors as determined by the material strength and forces applied to it. This may then be considered the optimal blade length and the integrated aerodynamic and structural design process would have run its course.

4.1. Structural design preamble

The blades must be able to function without failure at the pre-determined wind speeds and, therefore, their length is limited by the wind force's resulting stress. The structural design is thus the limiting factor in the size of the blades, as the aerodynamic design alone leads to an infinitely sized rotor, allowing to extract the maximum power from the wind.

4.1.1. Simple beam theory applied to rotor blade

In order to determine the normal and shear stresses working on the blade, basic beam theory was utilised for solving the shear and moment values at each section of the blade. This was done by modelling the rotor blade as a simple cantilever supported beam, with the forces acting on it determined by the thrust in the aerodynamic model.

The predetermined forces are applied to each section of the blade and an example of how these forces (designated one to ten) may look, as applied to the beam, are shown in Figure 17. Note that the thrust force is applied as a distributed load over the involved sections.

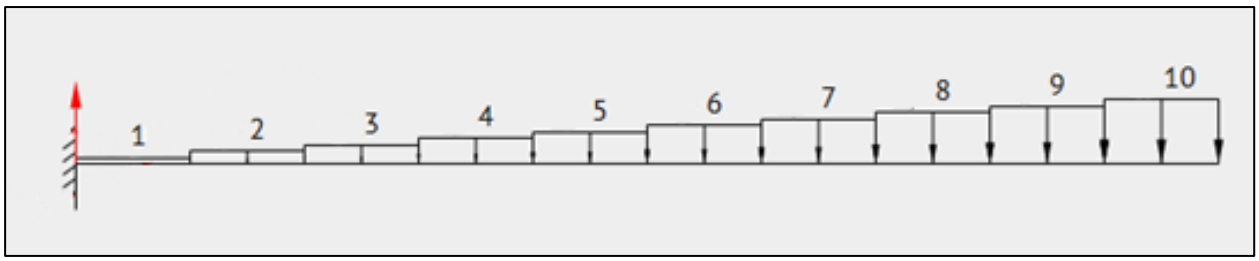

Figure 17: Sectional application of simple beam theory

In order to determine the stress for each section, the shear and moments are first determined. By first determining the support reactions, the shear and moment functions are found. From these functions, it is possible to find specific values for the shear and moment at each section.

To solve for the shear and moment functions, the following procedure (Hibbeler, 2013) is followed:

- Determine all the reactive forces and couple moments acting on the beam and then resolve these forces into components that act perpendicular and parallel to the beam's axis.
- Specify coordinates, designated with an *x*, that extend from the various sections that will have a distributed load applied to it, with no discontinuity between these coordinates for the length of the beam.
- Divide the beam into segments, as determined by the loads applied to it.
- Find the shear for each segment by tallying the forces perpendicular to the beam's axis.
- The moments are determined by tallying the moments at each segment's end.

- The resulting equations, in terms of *x*, can now be used, in conjunction with the known section lengths, to determine the actual shear and moment values for each section.

The shear and moment values can now be utilised in finding the stresses in the blade.

4.1.2. Driving forces acting on the blades

In this study three main stresses are considered. These stresses are induced by the rotation of the rotor (resulting in centrifugal driven stress) and thrust generated by the wind force (leading to shear and normal stress). The thrust is applied as a distributed load over the surface of the blade.

Due to the three-dimensional nature of the applied force on the blade, the forces are considered simultaneously. The centrifugal force, normal stress, and shear stress impact the sections concurrently and must be considered as a system. Consider the following simplification of the forces acting on the rotor:

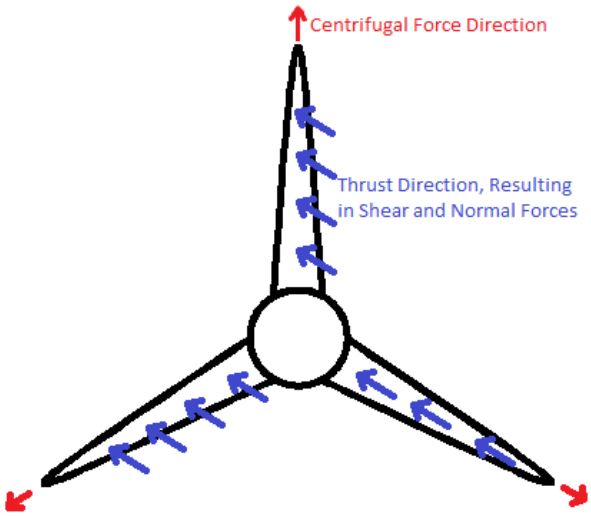

Figure 18: Simplified forces acting on rotor

When considering, in tandem, the magnitude of these forces and their directions of influence, the shear force is applied as a sole element as it alone is directed in the same direction as the thrust; while the centrifugal force and normal force combines to give a much larger stress concentration on the outer edges of the airfoil, both being directed outward from the centre of rotation.

The most prominent of these forces is the combination of the normal and centrifugal forces and resultant stress. The normal- and centrifugal force work in the same direction and is merely combined to determine the amount of stress the outer part of the blade will experience.

4.2. Stress factors

The entire model is integrated and written as functions of the input and output variables in order for the shape to solely be defined by the aerodynamic design and characteristics of the wind it harnesses. The length of the blade is determined by the material's structural characteristics and the stress applied to it. The full code can be found in Appendix A.

4.2.1. Centrifugal stress

As defined in Section 2.6.4, the first factor in the structural design process is the forces exerted by the rotation of the blade. The centrifugal forces acting on the blades depend on the weight and rotational speed of the turbine and the stresses for each of the sections can be analytically determined (RAENG1, 2014a).

4.2.2. Shear and normal stress

The primary force that affects the blade is the thrust generated by the wind. As it produces a distributed load on the blade, the wind generated thrust results in shear and normal stresses (Hibbeler, 2013). The shear formula is used to determine the stress the material undergoes while exposed to thrust, as described in Section 2.6.5.

The shear, normal, and centrifugal force-induced stresses – working in tandem – is used in the determination of the safety factors that limits the size of the blade.

4.2.3. Combined stress

Since the centrifugal- and thrust-related forces act simultaneously on the blade, the stress induced by these forces are superimposed in order to accurately predict the performance of the blades.

Figure 19 illustrates how the centrifugal force is directed away from the axis of rotation and how the resulting stress from this force may, therefore, be considered to work in the same direction of the normal stress at the blade section's outer edge.

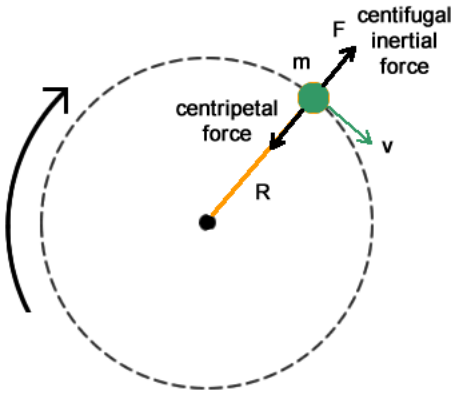

Figure 19: Illustration of centrifugal force direction

The normal and centrifugal forces work in the same direction, at the outside of the airfoil, and are tallied to determine the maximum force the airfoil will experience at its outer edge. When considering all the information (regarding the directions and applications of forces and the resulting stresses) for a section's outer edge, the total stress will therefore be a total of the normal and centrifugal stresses.

Considering the additional stress factors, the section's neutral axis is subject to the maximum shear force, with the maximum in-plane stress induced by a combination of maximum shear- and centrifugal forces. Figure 20 illustrates the distribution of these stresses.

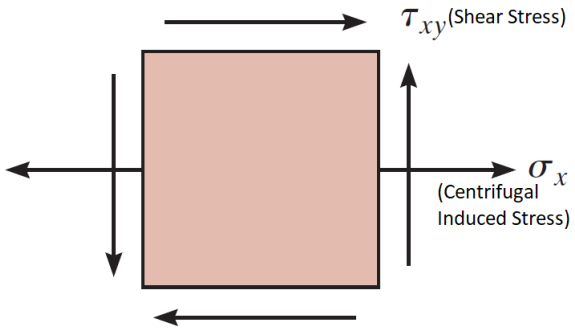

Figure 20: Stresses resulting in maximum in-plane stress (Hibbeler, 2013)

The following equation illustrates how the maximum in-plane shear stress is calculated:

$$\tau_{\max\,\text{in}-\text{plane}} = \sqrt{\left(\frac{\sigma_x - \sigma_y}{2}\right)^2 + \tau_{xy}^2} \qquad [26]$$

Since there are only two forces that attributes to shear stress in this instance, σ_y is zero, and is illustrated as such by its absence in the figure above.

The methods discussed are applied in the integrated design model and is elaborated upon in the next chapter.

4.3. Summary

Utilising the information and input from the aerodynamic design, the structural design phase illustrates how the blade is structurally evaluated to contribute to the final design process, along with the relevant forces exerted on the blade that is to be considered. Using the relevant methods, the structural design process hinges on a safety factor value that is deemed sufficient for the blade to withstand certain conditions. The structural and aerodynamic design processes are integrated to determine the final blade shape and characteristics.

CHAPTER 5 INTEGRATED MODEL DESIGN

In order to finalise the shape of the blade, the aerodynamic model is applied to determine the optimal blade shape. The structural model utilises the input from the aerodynamic model to scale the determined profile to a maximum length, whilst extracting the maximum power available from the regional wind conditions.

5.1. Material selection and properties

The manufacturing material selected for the design is polyethylene, since it is one of the most widely used plastics and especially suited for rotational moulding. Consequently, the material properties used in the integrated design process is derived from rotationally moulded polyethylene (Retief, 2015).

The material was subjected to physical testing to ascertain the suitability of the material properties when rotationally moulded.

To determine the effective density of the rotationally moulded polyethylene, samples were weighed, and their volume determined with the physical dimensions from a rectangular sample piece. The weight and volume of a sample can subsequently provide the density information required (Van der Walt, 2018).

Table 6: Material density measurements

Sample #	Length [mm]	Width [mm]	Height [mm]	Volume [mm^3]	Weight [gram]	Density [kg/m^3]
1	92	85	5	39100	26.1	667.5
2	87	80	6	41760	27.1	648.9

Table 6 indicates that the density used in the structural design, 650 kg/m^3, is close enough to the measured density to be used without expecting functional inaccuracies.

Conventional tensile testing on samples of polyethylene were conducted by using geometrically predefined samples and measuring the load at which the sample yields when subjected to a pulling force.

The following results were obtained (see Table 7 below) (Retief, 2015).

Table 7: Material tensile test results

Sample #	Yield Strength [MPa]
1	8.7
2	10.0
3	14.1

The yield strength used in the structural design process of 8.7 MPa is deemed to be conservative and as such it is suitable to use in the testing process for the safety factor evaluation. The actual performance of the rotor is therefore expected to be better than calculated in the integrated model; with it being able to handle higher wind speeds than predicted without failure.

5.2. Model input parameters

To determine the ideal blade shape, the following parameters (see Table 8) serve as the integrated design's input to solve for the blade geometry and length.

Table 8: Environmental input to model

Criteria	Value
Number of Blades	3
Air Density [kg/m^3]	1.225
Air Dynamic Viscosity [Ns/m^2]	0.00001831
Material Modulus of Elasticity [GPa]	2.3
Material Yield Strength [MPa]	8.7
Material Density [kg/m^3]	650
Hub radius [m]	0.2
Aerodynamic Design Wind Speed [m/s]	2.15
Maximum Gust Wind Speed [m/s]	17.5
Airfoil Thickness [mm]	7

The density and yield strength were determined by measuring the proposed rotationally moulded material (Retief, 2015) and by referencing known values for Young's modulus (The Engineering Toolbox, 2018). The airfoil thickness is taken as the maximum thickness that can be effectively rotationally moulded (Retief, 2015), as per the manufacturing process. This decision was made to simplify the design criteria. While it is possible to have a thinner airfoil skin, it will compromise the structural integrity of the blade. Using a thicker airfoil will result in the possibility of having to

adapt or change the manufacturing process. It will also increase the centrifugal forces exerted on the blade due to the higher mass of the blade.

From these input values, the model provides a solution to a suitable blade size that satisfies appropriate safety factors by iterative design. The blade length was adjusted to ensure that the blade satisfies safety factors and can withstand sudden gust conditions at 17.5 m/s.

5.3. Premise of combined model's solution

The structural solution is based on appropriate safety factors. The safety factor for gust conditions, as previously calculated, is chosen as 1.05. Therefore, the design of the blade is based on the premise that it can withstand gust wind forces at 17.5 m/s with a safety factor of approximately 1.05. The blade length is thus determined by this safety factor for wind speed at gust conditions.

The aerodynamic solution is based on an optimum wind speed of 2.15 m/s, as shown by the optimisation method for aerodynamic wind turbine design. The power per year is maximised by using this wind speed and optimising the aerodynamic wind turbine blade design for this wind speed will therefore result in the highest kW delivered per year for the selected geographic area. The optimisation of the blade is done by altering the pitch angle of each section to increase the effective torque delivered per section, as power is a function of torque.

The total optimisation of blade length and changing of the pitch angle per section is done by iteration, until the proposed blade length no longer meets the required safety factors.

5.4. Model output summary

Table 9 indicates the results of the integrated model as fully defined and illustrated in Appendix A, following the iterative integrated design process.

Table 9: Final blade design results summary

Design Wind Speed	Design Rotational Speed	Blade Length	Design Power	Minimum Safety Factor
2.15 [m/s]	43 [RPM]	2.4 [m]	56.28 [W]	1.066

In order to find a suitable solution to the blade geometry, the initial blade geometry – as defined by the aerodynamic design – was scaled and increased in size until the design could no longer withstand the stress induced by the rotor's operation as determined by the properties of the rotationally moulded plastic. As the blade length is increased, the stress along the blade's length

is increased and the effective safety factors per section decreases until any further elongation of the blade will result in failure under gust-wind conditions.

The final design's safety factor of 1.066 was deemed sufficient for the area's maximum gust-wind conditions, as it would be redundant to restrict the blade length further for exceptional conditions that, statistically, are highly unlikely to occur. See Appendix A for full calculations and results.

5.5. Final blade geometry

By considering the results from the integrated model and applying the determined geometry to a 3D model, the drawing in Figure 21 illustrates the characteristics of the final manufactured blade.

In addition, Appendix B features additional drawings for the final blade geometry and characteristics.

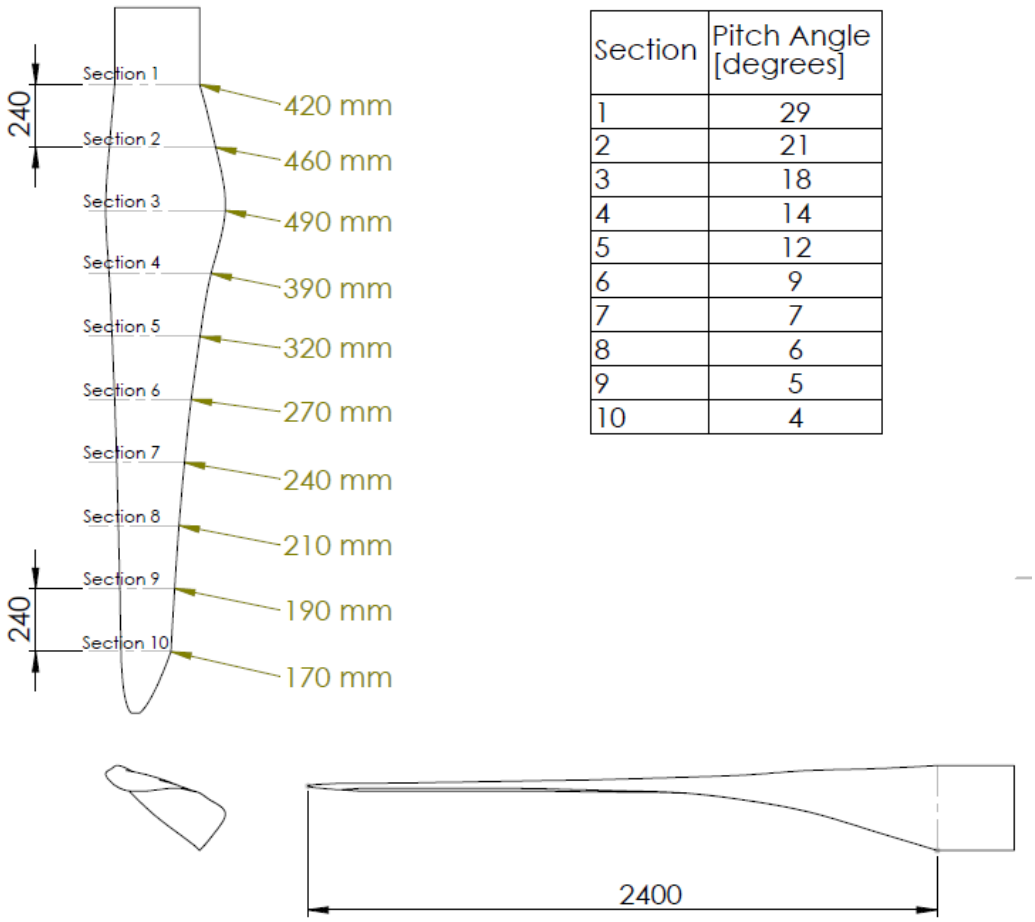

Section	Pitch Angle [degrees]
1	29
2	21
3	18
4	14
5	12
6	9
7	7
8	6
9	5
10	4

Figure 21: Final 2D blade design drawing

As depicted, the rotor blade is similar to conventional turbine blade designs.

5.6. Summary

The structural and aerodynamic methods are integrated to determine and fix the ideal blade shape, size and geometry. The final blade design is deemed to be the best suited to maximise the annual power output for low wind speed areas such as those found in the Potchefstroom region.

CHAPTER 6 VERIFICATION AND VALIDATION

This chapter details the verification and validation of the aerodynamic and structural design process in order to ensure that modelling was done accurately and that the methods are valid to use when designing a wind turbine rotor.

6.1. Aerodynamic verification and validation

The aerodynamic model is verified and validated in order to confirm that the model's implementation is accurate in order to ascertain the performance parameters of a manufactured turbine in operating conditions.

6.1.1. Verification of the BEM's implementation

The aerodynamic model is verified to confirm whether the BEM was implemented correctly by comparing the model's results with results from PROPID simulation software (Bosman, 2003). The same environmental conditions are applied for both the model and tested rotor. If the results from the aerodynamic model and PROPID corresponds it will demonstrate that the implementation of the BEM in the aerodynamic model was done correctly.

The results from the aerodynamic model which made use of the blade momentum theory, is compared with results from an alternative source by using PROPID that utilised the same input. The following graph and data obtained from the aforementioned is used.

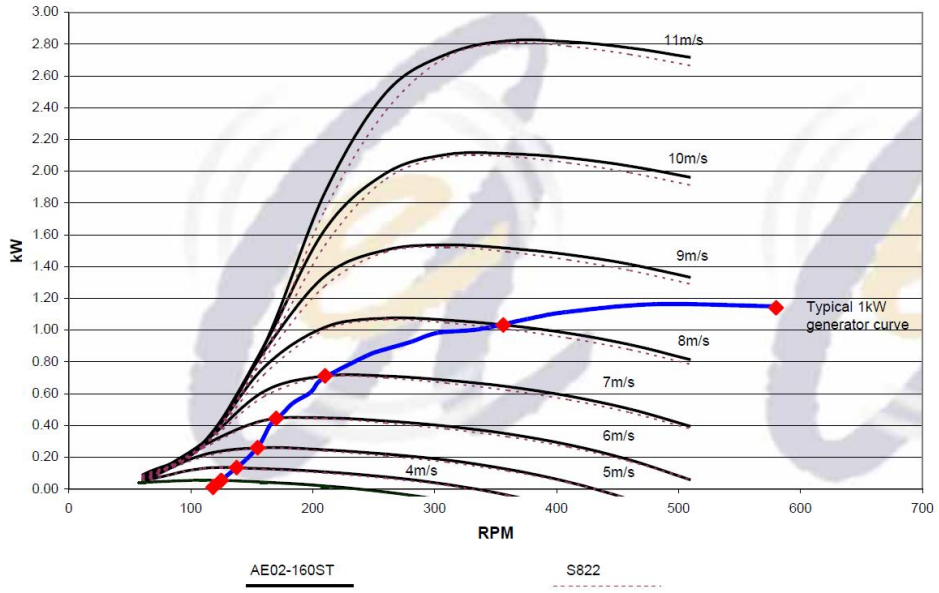

Figure 22: Blade curves for airfoil used in design (AE02-16ST) (Bosman, 2003)

Table 10 indicates the environmental specifications for the above-mentioned blade. These same specifications serve as the input to the aerodynamic blade momentum theory-based model.

Table 10: Environmental input to model verification

Factor	Value
Blade Length [m]	1.8
Number of Blades	3
Air Density [kg/m^3]	1.2
Dynamic Viscosity [Ns/m^2]	1.8 E-05
Twist Range [degrees]	4 to 29

To determine whether the model provides accurate results the same blade specifications are used in the testing and comparison of the model against those simulated (see Table 12). The exact twist of the tested blade for each section of the blade is not known and was assumed to be evenly distributed across the blade length as shown in Table 11.

Table 11: Blade specifications for verification of model

Chord Length [m]	Pitch Angle [deg]
0.136	29
0.136	21
0.136	18
0.124	14
0.112	12
0.100	9
0.092	7
0.084	6
0.072	5
0.068	4

Using the above input, the tested blade used for the verification process's results (as shown in the aforementioned blade curves) provided data shown in Table 12, which is compared to results obtained from the aerodynamic model. The wind speeds ((4 – 6 m/s) and RPM (100 and 150)) were chosen to be used in the comparison process, as it falls within in the range that the turbine is expected to operate (as discussed in Section 3 of this study).

The following table illustrate the results from the model and PROPID sourced blades.

Table 12: Comparison of model's results and sourced blade's results

Wind Speed [m/s]	RPM	Power Output [Model]	Power Output [PROPID Blade]	Difference [%]
4	100	128.31	115	11.6%
	150	118.91	140	-15.1%
5	100	172.67	190	-9.1%
	150	286.12	255	12.2%
6	100	184.3	225	-18.1%
	150	453.59	410	10.6%
			Average Absolute Difference	12.8 %

The above results are deemed sufficiently accurate for the model to be used in the proposed design of the wind turbine blades. The inaccuracies may be attributed to the known inaccuracy of the blade momentum theory's disregard of secondary effects, such as those induced by the radial components of flow (Auld & Srinivas, 2017).

The model is therefore deemed fit to accurately implement the Blade Element Method.

6.1.2. Validation of the BEM's ability to simulate real world performance

In order to validate the use of the BEM in the aerodynamic model, the model's predicted results are compared to results obtained from an experimentally tested wind turbine blade. Comparing the experimentally measured power coefficients with the predicted power coefficients from the aerodynamic model will confirm whether the model is suitable for use in predicting the real world performance of the rotor. Validating the model will confirm the correctness of its predication of performance instead of reverting to experimental measurements every time input parameters are changed.

The model is compared to a wind turbine rotor tested in a wind tunnel (Hsiao, 2013), which has optimised blade taper and twist distributions so as to provide better efficiency over a wider range of tip speed ratios. The referenced blade's power production was measured experimentally in a wind turbine tunnel and related to power coefficient, which is then compared to the power coefficient prediction of the mathematical aerodynamic model.

The same input parameters was used in the mathematical model with regards to blade geometry and environmental conditions. The following table denotes the input parameters and characteristics of the tapered and twisted optimised tested blade (OPT setup).

Table 13: Experimentally Tested Rotor Characteristics

Design Parameter	Value
Rated Power [W]	50
Rated Wind Speed [m/s]	10
Design Tip Speed Ratio	5
Number of Blades	3
Design angle of attack [°]	5.5
Airfoil Type	NACA4418
Rotor Diameter [m]	0.72

In addition to the design characteristics of the optimised blade, the following geometry is imported into the Blade Element Theory aerodynamic model, as per the referenced optimised blade experimentally tested.

Table 14: Experimentally Tested Rotor Twist and Chord Characteristics

Section	Chord Length [m]	Twist Angle [°]
1	0.096	25.92
2	0.085	17.56
3	0.072	12.20
4	0.061	8.61
5	0.053	6.08
6	0.046	4.21
7	0.041	2.78
8	0.036	1.65
9	0.033	0.75
10	0.030	0.00

By using the input defined in the previous two tables in the Blade Element Theory based model along with data generated with XFoil with regards to lift and drag for the specific airfoil, the experimental results from physically testing the rotor can be compared to the aerodynamic model's prediction of power output. This will serve as a check to ensure that the mathematical model will realistically simulate real world performance, and that it may therefore be used in the design process of the cost efficient wind turbine rotor.

The performance of the experimentally tested blade is measured in terms of C_p (coefficient of performance), as the goal of the referenced experiment is to determine the effect on efficiency various changes to the blades geometry will have. Therefore, the aerodynamic model's results is also converted to a C_p value for comparison using the following formula (Hsiao, 2013).

$$C_p = \frac{P_m}{0.5\,\rho\,R^2\,V^3} = \frac{T_m \omega}{0.5\,\rho\,R^2\,V^3}$$

Where

C_p = Coefficient of performance
P_m = Mechanical power [W]
T_m = Torque [N.m.]
ω = Rotational Speed [rad/s]
ρ = Air density [kg/m^3]
R = Rotor radius [m]
V = Wind speed [m/s]

The following table illustrates the aerodynamic model's results as per the input conditions specified.

Table 15: Aerodynamic Model's prediction

Rotor RPM	Tip speed ratio	Power Production [W]	C_p
796	3	69.80	0.274
928	3.5	100.39	0.395
1061	4	128.74	0.506
1194	4.5	136.45	0.536
1327	5	127.68	0.502
1459	5.5	107.99	0.424
1592	6	98.61	0.388
1724	6.5	87.86	0.345

The table above illustrates the predication that highest efficiency is around the design tip speed ratio, with the effectivity reduced at tip speed ratios further from the design ratio.

The following graph illustrates results obtained from experimentally testing the three blades, with "OPT" denoting the optimum blade setup (and the setup used for comparison with the aerodynamic model), "OUT" denoting an untapered but optimally twisted setup, and "UUT" being an untapered and untwisted blade setup.

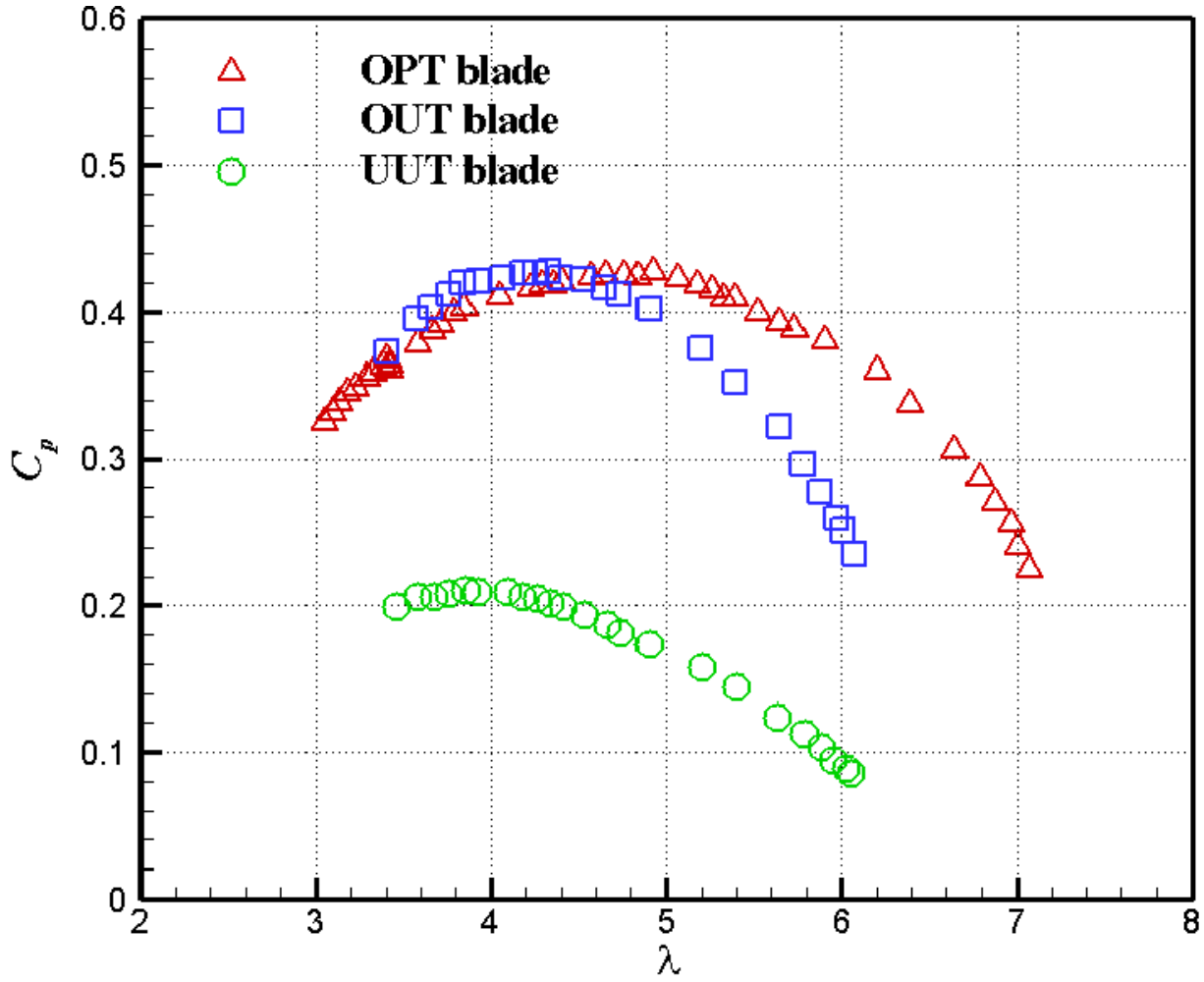

Figure 23: Tip speed ratio vs C_p blade experimental results

From the above graph it is clear that optimising the blade taper and twist will lead to better efficiency over a wider range of rotor speeds.

For the evaluation of the aerodynamic model's ability to accurately simulate real world results, the aerodynamic model's results are compared with the OPT blade setup as shown in the following graph.

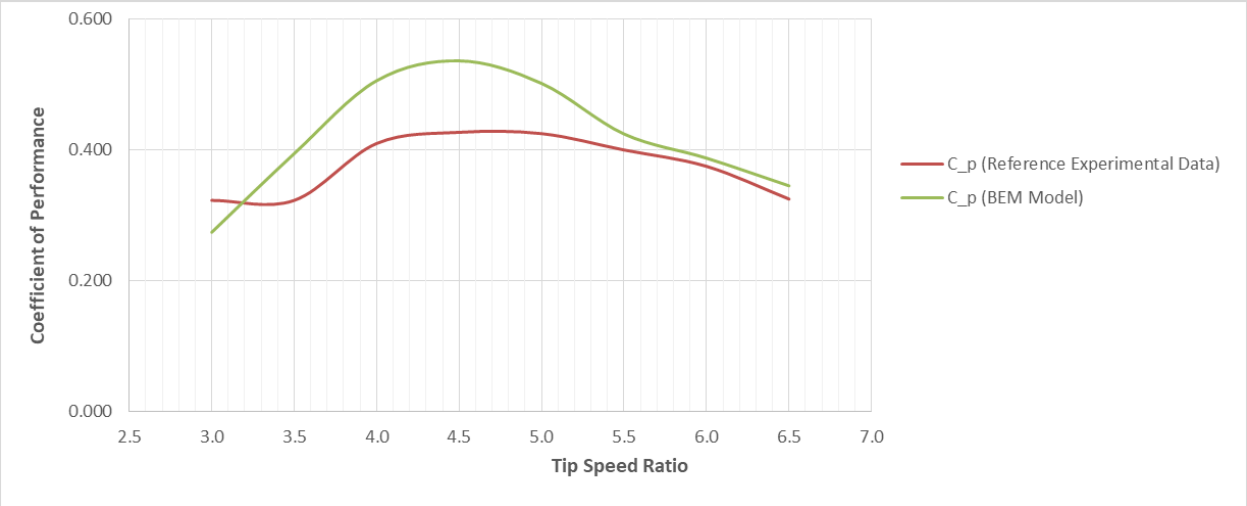

Figure 24: Aerodynamic Model and Experimental Results comparison graph

From the above graph it can be deduced that the aerodynamic model over-predicts the efficiency of a turbine rotor compared to the real world results.

The following table illustrated the percentage differences in results as per the above graph.

Table 16: Aerodynamic Model and Experimental Results comparison table

Tip Speed Ratio	Experimental Cp	Model Cp	% Difference
3	0.323	0.274	-15.1%
3.5	0.376	0.395	22.1%
4	0.410	0.506	23.4%
4.5	0.434	0.536	25.6%
5	0.440	0.502	18.1%
5.5	0.425	0.424	6.1%
6	0.400	0.388	3.3%
6.5	0.370	0.345	6.2%

Using an improved BEM method which incorporates stall models and tip loss factors should improve the correlation between real world and predicted results. The discrepancies between the experimental data and predicted results may also be attributed to the neglected 3D flow velocities and tip vortex or radial components associated with the rotation of the turbine during operation neglected by the BEM method.

From the comparison between the experimental results and the predicted results from the aerodynamic model, the aerodynamic model is validated to predict real world performance accurately enough to in order to find a suitable size of a wind turbine in low wind speed areas, and will therefore be effective in the design of a wind turbine rotor as proposed in this study.

6.2. Structural analysis verification and validation

In order to verify and validate the structural design process, finite element method analysis was applied. Using a software-based FEM (Finite Element Method) evaluation, the beam theory-based design can be evaluated, firstly in order to verify whether the structural analysis of the blade was implemented correctly, and secondly to validate that the structural analysis' results correlate with the actual performance of a manufactured wind turbine blade.

6.2.1. Examination of FEM analysis software

To evaluate the 3D model as determined by the integrated design process, the software package ANSYS (2018) was used. With ANSYS, simulations were performed on the model and thus provided data for comparison to the simple beam-theory based calculations, as per the structural design process discussed in previous chapters.

The accuracy of FEM analysis, also referred to as FEA (Finite Element Analysis), compared to real-world results, depends on a number of factors that include (Visser, 2014):

- The similarity of the material properties of the real-world structure and the material properties entered into the simulation software.
- All relevant physics relating to real-world effects must be considered in the software simulation.
- Loads and load distributions must be accurately applied in the simulation setup.
- Constraints and boundary conditions must be identical as to how the real-world structure will be applied in practise.
- The simulated 3D model must be identical to the real-world structure's geometric representation.

When considering the factors contributing to the real-world accuracy of FEA evaluation, simple and singular components – with simple loads applied – will yield accurate results easier than complex structures with integrated load conditions (Visser, 2014).

The validity of a FEM analysis's results depends on the ability of finite element methods to replicate experimental results. Prior to considering the accuracy of the method, the method itself must be considered as valid for verifying the expected results obtained during experimental testing. Due to the heightened capability of computers and related software, modern FEA is increasingly used to optimise designs before commencing manufacture.

For this study to incorporate FEM analysis as a valid method to compare with the analytical model's results, the application of this method is compared with experimental results from various sources in order to ensure its validity (Mullen, 2018).

Table 17 indicates the correlation between some relevant literature that used FEM analysis and compared their results with the experimental results, in order to illustrate how increasingly modern FEM analysis typically have higher accuracy. It is assumed that the aim of the cited FEM analyses was to achieve results that simulate realistic performance and that the recorded experimental procedures were setup optimally (Mullen, 2018).

Table 17: Comparison of FEA to experimental results according to software age

Year	Author(s)	Difference between FEM and Experimental results
2007	Wood *et al.* (2007)	8 %
2010	Duan *et al.* (2010)	5 %
2014	Hsu *et al.* (2014)	3 %
2017	Kan *et al.* (2017)	1 %

When considering the accuracy of the cited FEA software packages, Table 17 illustrates the quality of analysis has increased during the past decade. To further illustrate how using modern FEM software with modern computer technology provide an accurate method of predicting real-world results, the analysis of a 5kW wind turbine is now examined (Sami *et al.*, 2014).

6.2.2. Comparing FEM analysis and real world performance

In an analysis of a 5kW wind turbine blade by Sami *et al.* (2014), a glass reinforced polyester composite blade was analysed in the software package ANSYS Multiphysics (ANSYS, 2013) and compared to results from experimental testing. The finite element model was statically validated by means of experimental results and the FEM analysis was found to accurately predict real-world results, as obtained by experimental testing. The blade had the following design characteristics:

Table 18: 5kW validated blade characteristics (Sami *et al.*, 2014:84)

Parameter	Unit	Value
Power Rating	[kW]	5
Blade Length	[m]	2.67
Maximum Chord Length	[m]	0.372
Maximum blade twist	[deg]	19.7
Airfoil	[-]	S809

The following results were obtained during static structural testing of the blade and was compared to results obtained from the ANSYS analysis.

Table 19: 5kW validated blade FEA and experiment results (Sami *et al.*, 2014:84)

Parameter	Unit	FEM Result	Measured Result	Deviation
Applied Load (Flapwise)	[kg]	37	37	-
Applied Load (Edgewise)	[kg]	37	37	-
Deflection (Flapwise)	[mm]	111	99.11	10.71 %
Deflection (Edgewise)	[mm]	33	29.15	11.67 %
Longitudinal Strain	[-]	3258	3119	4.27 %
Transverse Strain	[-]	641	469	26.83 %

Considering the results and the possibility for errors when setting up experimental testing, and the fact that the study was done in 2014 with software that was available that year, the experimental results are deemed to conform to the prediction by the FEM analysis. Furthermore, the tested blade has similar characteristics than that of the final design of the blade in this study. It may therefore be assumed that the software package's latest version, ANSYS 19.0 (2018), as used in this study, will accurately predict results of the blade's real world performance as per the design set out in the previous sections of this study.

Taking the previously discussed accuracy of FEA methods into account, it is deemed possible to accurately model the blade with regards to real-world performance. However, when comparing the accurate FEM analysis of the blade to the simplified beam theory-based structural analysis – used in the integrated design model –at least some inconsistencies are expected in the results. While care has been taken to build a beam theory based model that will represent the true three-dimensional nature of the wind turbine blade, the beam theory is expected to be less accurate than the FEM based analysis when compared to the real-world performance of the blade.

When the FEM analysis, analytical methods and real-world performance are compared, differences may be as large or small as times larger or ten times smaller (one order of magnitude). This may be the case when the many possible variations in the setup of the FEM model and the obvious limitations of using simple beam theory to predict the performance of a three-dimensional problem, are considered (Mendez, 1999; Panagiotopoulou *et al.*, 2012; Visser, 2014).

When proper care is taken in accurately setting up the FEM simulation, and the beam theory-based analytical solutions are accurately modelled to match the geometry and properties of the structure, the achieved results' accuracy are greatly increased. In using complex boundary

conditions, exact geometric modelling, beam theory-based analysis and FEM analysis, solutions with less than 5% difference may be achieved (Blasques *et al.*, 2016; Faccio, 2017).

Considering the simplicity of the beam theory analysis used in the integrated model and the accuracy of FEM software, the results from the beam theory and FEM analysis are expected to correlate but with some deviation expected.

6.2.3. FEM setup for analysing wind turbine blade and structural model

In order to analyse the rotor blade, the engineering simulation software package ANSYS (2018) was used to determine whether the beam theory based structural analysis model was implemented correctly, and secondly to determine whether the use of this method is valid for the structural analysis of a blade. If the results from the FEM analysis corresponds with that of the beam theory based model, the method will be deemed both verified and validated.

The forces from the MS Excel-based aerodynamic model was applied to a three-dimensional model using ANSYS's structural analysis tools. The results were compared to the structural results from MS Excel. The forces applied were the thrust and centrifugal forces, due to the rotation of the blade during operation. The scenario used in the analysis considered the blade operating at the design wind speed of 2.15m/s and a blade length of 2.05m. If the structural results from the MS Excel model and the ANSYS analysis correspond, it may be assumed that the structural analysis methodology is accurate and valid.

For the analysis, a lower wind speed is chosen because it is expected to deliver results better simulating realistic conditions, since the possible deformation of the blade during higher wind speed may negate the effectivity of the beam-based model which does not explicitly take deformation characteristics into account. Keeping the comparison between two highly similar scenarios is an effective way to regulate uncertainties and unknown boundary conditions.

Initiating the model's setup in ANSYS, the density and modulus of elasticity were imported into the model, as described in previous chapters. A 3D model was imported and set as a shell arrangement, with a thickness in accordance with the 10mm used in the beam theory model.

Table 20 denotes the loads as applied to each section of the 3D model in ANSYS, as per the MS Excel based aerodynamic model's thrust deliverables.

Table 20: Load specifications for ANSYS FEM analysis

Section	Load [N]
1	1.31
2	2.60
3	3.68
4	4.13
5	4.26
6	5.40
7	6.18
8	7.01
9	8.07
10	8.68

The above loads were applied per section of the 3D model, as described for the beam theory-based model.

Additionally, the blade was subjected to a rotational speed of 46 RPM or 3.82 rad/s, with the rotational factor delivering the centrifugal force acting on the blade.

In order to extract results from the simulation, control areas were designated on the 3D model that correspond to the sectioned areas of the beam theory. From this, the maximum stress could be interpreted in table form. The simulation was set up in such a manner that results obtained can be compared to the combination of normal and centrifugal forces, as this combination was seen to be the driving stress in the beam theory analysis. The following figure illustrates the control areas designated.

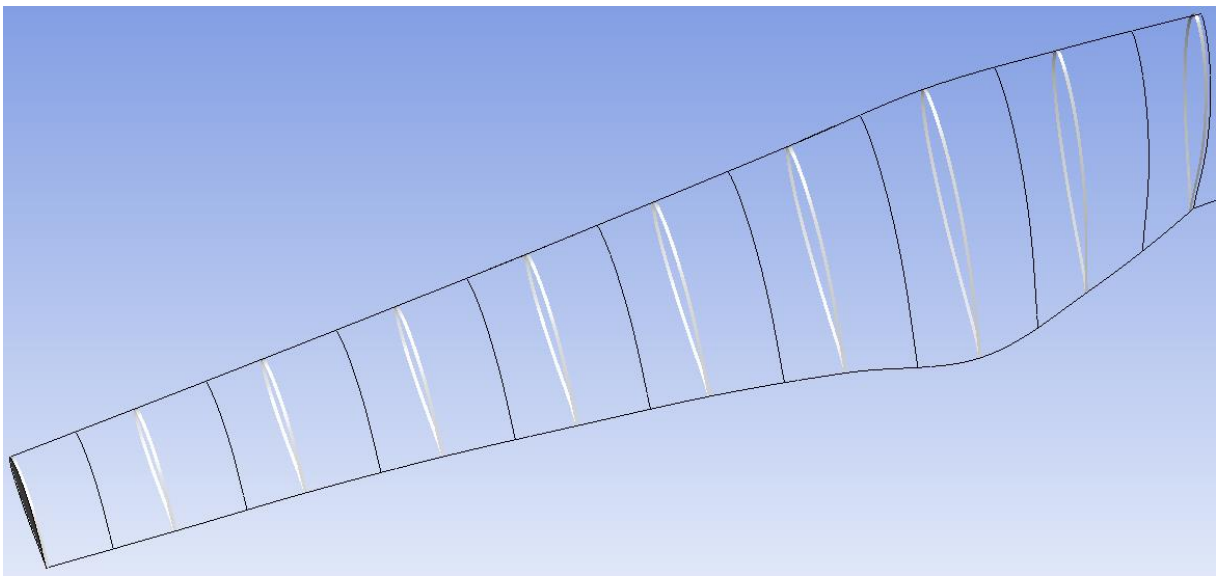

Figure 25: Control areas - shown as silver bands – used as reference during FEM analysis

To verify and validate the beam theory-based structural analysis, the results per section of the FEM analysis can now be compared to the beam theory model's results.

6.2.4. FEM analysis results

Figure 26 illustrates the simulated rotor blade. The maximum stress concentrations are in areas toward the base of the blade, with the tip of the blade having the least effective stress.

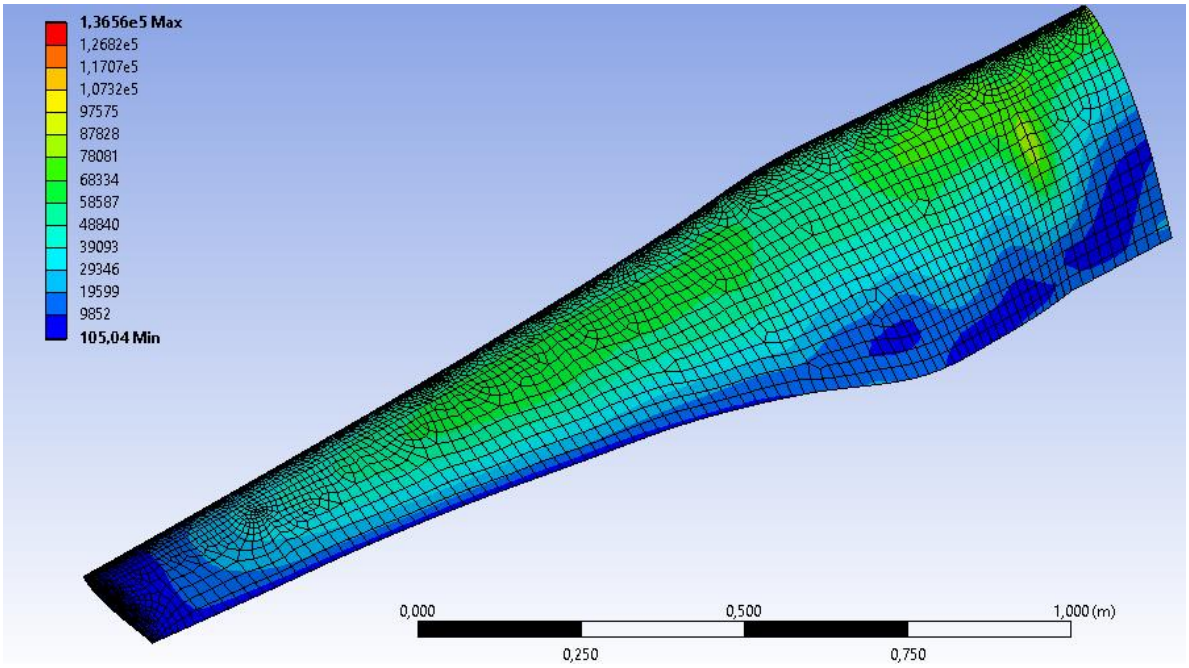

Figure 26: FEM analysis model results

It is evident that the trailing edge and blade tip areas are effectively the least exposed, while the leading edge and centre of the blade experience higher stress concentrations.

The results from the FEM and beam theory models are compared in Table 21.

Table 21: FEM analysis results

Section	FEM Results [Pa]	Beam Theory Results [Pa]	% Deviation
1	94 305	111 666	-15.5
2	67 285	84 297	-20.2
3	55 490	64 290	-13.7
4	67 636	71 237	-5.1
5	62 431	72 133	-13.4
6	67 193	67 260	-0.1
7	59 429	55 895	6.3
8	43 964	39 968	10.0
9	23 318	22 589	3.2
10	5 276	8 038	-34.4

The deviation of results between the FEM analysis and Beam Theory based calculations vary up to about 20%, with an outlier of 35% deviation at the outer tip section. However, when considering the factors mentioned in previous sections, regarding the accuracy of beam theory when compared to FEM models, the difference falls within the expected scope of deviation.

The following graph gives a visual interpretation to the above results.

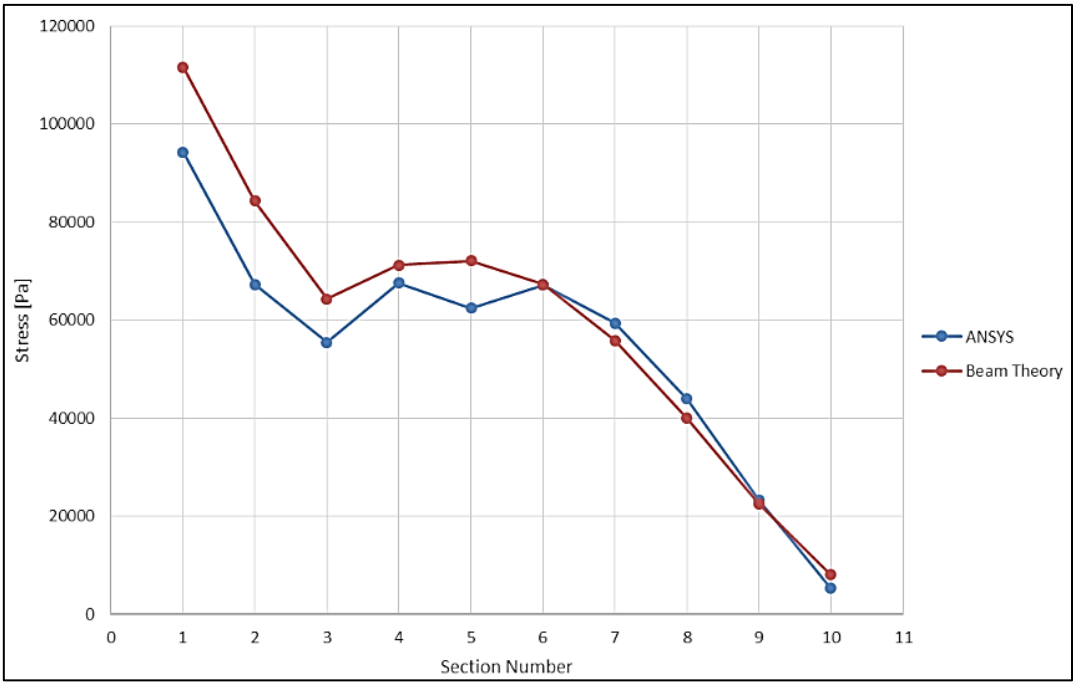

Figure 27: Graph comparison of FEM and beam theory results

As illustrated, the two models follow the same trend. The FEM model shows an irregularity at Section 5, which may be attributed to a number of factors. It may be due to a geometric anomaly in the 3D shell model, mesh distribution, numerical irregularity in the convergence of the FEM solution, or other related issues.

6.2.5. Confirming mesh independence of FEM analysis

In order for the results of a FEM analysis to be acceptable, mesh independence must be confirmed. Mesh independence refers to the state where a refinement or increase in the number of elements or nodes of the applied mesh, will not result in a significant change in the results obtained from the simulation (De Kock, 2013).

This implies that the mesh is gradually altered to produce increasing elements, until successive results from the analysis do not significantly differ. The acceptable degree of difference per successive results are driven by the convergence of the solution and the associated time taken to solve the FEM analysis (LEAP CFD Team, 2012). Solutions with a high number of elements take longer to solve and absolute element independence will generally be accompanied by very high element and node counts. To determine whether mesh independence is reached, the percentage difference between successive results are compared with the maximum and minimum stress along the rotor blade for each simulation being compared.

Table 22 denotes the stress results as the mesh size is decreased.

Table 22: Stress results for decreasing mesh size

Number of Elements	Maximum Stress [Pa]	Minimum Stress [Pa]
19211	94305.4	5298.5
16650	93388.5	5297.3
14605	92505.9	5298.4
12414	93646.6	5303.5
9707	94533.4	5312.8
8135	96157.8	5251.8
6699	92802.8	5242.8
4411	97048.7	5264.6
3094	95771.2	5327.7
2074	91781.6	5294.7
1470	87699.4	5386.8

Table 23 denotes the change in results as the number of elements are increased.

Table 23: Mesh independence test results

Change in Elements		% Difference	
From	To	Maximum Stress	Minimum Stress
16650	19211	0.98%	0.02%
14605	16650	0.95%	0.02%
12414	14605	1.54%	0.10%
9707	12414	0.94%	0.18%
8135	9707	1.69%	1.17%
6699	8135	3.62%	0.16%
5349	6699	4.37%	0.04%
3094	4411	1.33%	1.18%
2074	3094	4.35%	0.62%
1470	2074	4.65%	1.71%

The results in the table are plotted to illustrate the absolute percentage change for successive results, as the number of elements in the FEM analysis is increased.

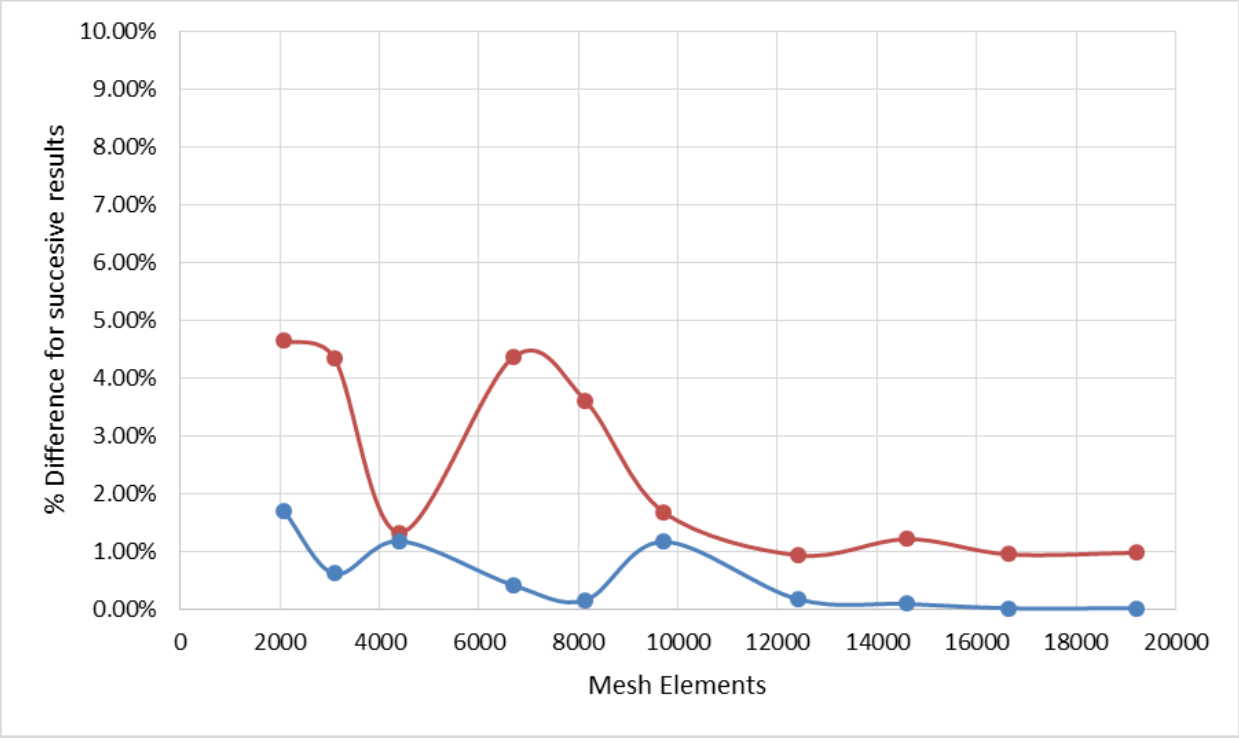

Figure 28: Mesh independence test results

As the number of elements are increased, it is evident that change in successive results decreases. The changes for the maximum and minimum stresses for successive results, of less than one percent, are deemed sufficient to prove that mesh independence is reached. The FEM

results used to verify the analytical beam-based theory, as discussed in previous sections in previous chapters, were done with 19211 elements, and is deemed mesh independent.

6.2.6. Verification of structural model

Considering the FEM results in the previous sections and Table 21, the beam theory based solution's results corresponds with the results from the FEM analysis with the deviation of results falling in the expected range of inaccuracy. The implementation of the beam theory based analysis method is therefore verified to be correctly implemented and accepted.

6.2.7. Validation of structural model

With reference to Section 6.2.2. the results obtained from modern FEM software solutions sufficiently replicate real world performance as described by the comparison of the 5kW wind turbine blade's experimental results and FEM results. The comparison demonstrates that FEM results accurately simulate real world conditions when care is taken to set up the analysis correctly.

The correspondence of the beam theory based solution's results and the FEM analysis performed in this study therefore confirms that the use the beam theory methodology is a valid way to analyse the structural performance in the design of a wind turbine blade as proposed in this study, with the structural model effectively predicting real world performance.

6.3. Summary

This chapter aimed to verify and validate the integrated aerodynamic and structural model, and did so by comparing the aerodynamic section of the model with results from a simulation software package and a blade that was subjected to experimental testing. By applying the Excel based aerodynamic model to an identical setup as the experimentally tested blade, similar results were obtained as with the simulation package and physical testing. The structural analysis was also effectively verified and validated by comparing the beam-theory based solution to a FEM analysis of the 3D model. The material tests were also useful to determine the validity of the assumed material properties and imported to the integrated design model.

It can therefore be concluded that the integrated model is an effective method to analyse and estimate the maximisation of a wind turbine blade length and subsequent power production for lower wind speed areas.

CHAPTER 7: CONCLUSION AND RECOMMENDATIONS

7.1. Conclusion

The use of analytical and statistical methods to determine the most efficient geometry and characteristics of a wind turbine rotor – for the low wind speeds commonly found in inland South Africa – is deemed accurate and efficient enough to base a design on that may be used to manufacture a wind turbine rotor's blades with rotational moulding. Considering the material characteristics of rotationally moulded polyethylene and the annual wind data for Potchefstroom in South Africa's North-West Province, the aerodynamic blade element theory can be combined with a beam theory-based structural analysis, to produce an estimation of the ideal rotor size. The input for this integrated model involved matching Weibull distributions to real historical data for the wind speed in the chosen region and then finding the ideal design wind speed to maximise the power production per year.

The methods described in Chapters 3 to 5 concluded that a rotor with a blade length of 2.4 meters would be ideally suited to operate at a design wind speed of 2.15 meters per second, and able to withstand gust-wind conditions at 17.5 meters per second without failure. Chapter 6 sought to verify and validate the results from the analytical methods, by means of FEM analysis and by comparing the results from the aerodynamic model with known results of a similar blade that was physically tested.

With the results from the verification methods, the model is deemed accurate in the methods used and the results obtained can therefore be considered true and correct.

7.2. Recommendations

It is recommended that the analytical model used in the determination of the rotor blade's size and geometry be integrated with computer-based tools such as CFD and FEM to a much greater extent in order to achieve more accurate results and performance predictions. The simplicity, speed and ease that make simple analytical methods popular to use, is outweighed by the accuracy of numerical methods, which are therefore recommended to be used more integrally in the design and modelling of a rotor blade.

Further analysis with computer-based tools may also be necessary to determine the deformation of the rotor blades at very high wind speeds to ensure sufficient clearance from the tower that the rotor is mounted on and, also, the effect the deformation has on the performance and power generation capabilities of the rotor.

It may also be prudent to do a vibrational analysis on the chosen material and on the rotor, to determine whether the design conditions are valid and whether dampeners should be included in the design of the tower, wind turbine blades, and nacelle.

Finally, in order to increase the effective rotor diameter and subsequent power output, the internal reinforcement of the blades by inexpensive means may be investigated. This might include the addition of simple aluminium beams moulded into the centre of each blade, thus allowing for higher stress tolerances. It may also increase the allowable length per blade without adding a considerable amount of weight to the blades. Adding these reinforcements will undoubtedly increase the power output without a considerable increase in the manufacturing cost.

REFERENCES

Al-Shemmeri, T. 2010. Wind turbines. London: Bookboon.

Andres, R.M. 2016. Betz limit. http://www.reuk.co.uk/Betz-Limit.htm Date of access: 14 Mar.

ANSYS. 2013. Fluids simulation advancements in ANSYS 15.0 bring faster and more accurate results to users. https://www.ansys.com/about-ansys/news-center/12-20-13-fluids-simulation-advancements-in-ansys-15-0 Date of access: 10 Nov. 2018.

ANSYS. 2018. Multiphysics. https://www.ansys.com/products/platform/multiphysics-simulation Date of access: 10 Nov. 2018.

Auld, D.J. & Srinivas, K. 2017. Blade element rotor theory. http://www.aerodynamics4students.com/propulsion/blade-element-rotor-theory.php Date of access: 21 Dec. 2018.

Blasques, J.P., Bitsche, R.D., Fedorov, V. & Lazarov, B.S. 2016. Accuracy of an efficient framework for structural analysis of wind turbine blades. *Wind Energy*, 19(9):1603-1621 doi:10.1002/we.1939

Bosman, J.J. 2003. The aerodynamic and structural design of a 1kW wind turbine blade. Paper presented at the World Wind Energy Conference, Cape Town, South Africa, 23-26 Nov.

BPF (British Plastics Federation). 2018. Rotational moulding. http://www.bpf.co.uk/plastipedia/processes/Rotational_Moulding.aspx Date of access: 22 Jun. 2018.

Caboz, J. 2018. These are the 5 biggest green energy projects in SA - all wind farms. *Business Insider South Africa*, 6 Apr. https://www.businessinsider.co.za/5-massive-new-renewable-energy-projects-that-transformed-south-africas-landscape-2018-4 Date of access: 11 Nov. 2018.

Chatott, J.J. 2003. Optimization of wind turbines using helicoidal vortex model. *Journal of Solar Energy Engineering*, 125(4):418-424 doi:10.1115/1.1621675

Cvitan, L. 2003. Determining wind gusts using mean hourly wind speed. *Geofizika*, 20:63-73.

De Kock, R. 2013. Mesh independence. *ESTEQ Engineering Solutions*, 12 Jun. https://esteq.co.za/2013/06/12/mesh-independence/ Date of access: 5 Oct. 2018.

DiFrangia, M. 2014. A brief specification for a complete blade monitoring system. *Windpower*, 4 Mar. http://www.windpowerengineering.com/design/mechanical/blades/brief-specification-complete-blade-monitoring-system/ Date of access: 27 Mar. 2016.

DNV/Risø (Det Norske Veritas/Wind Energy Department - Risø National Laboratory). 2002. Guidelines for design of wind turbines. Copenhagen, Denmark: Authors. http://www.homepages.ucl.ac.uk/~uceseug/Fluids2/Wind_Turbines/Codes_and_Manuals/Guidelines_for_Design_of_Wind_Turbines.pdf Date of access: 27 May 2017.

DoE (Department of Energy). 2015. State of renewable energy in South Africa. Pretoria: Government printers. http://www.energy.gov.za/files/media/Pub/State-of-Renewable-Energy-in-South-Africa.pdf Date of access: 10 Nov. 2018.

DoE (Department of Energy) ***see*** South Africa. Department of Energy.

Duan, C., Cai, Y. & Li, Y. 2010. Finite Element Simulation and Experiment of Chip Formation during High Speed Cutting of Hardened Steel. *Applied Mechanics and Materials*:29-32.

Faccio, C.J.J. 2017. Modelling wind turbine blades by geometrically-exact beam and shell elements: a comparative approach. São Paulo: University of São Paulo. (Thesis - Masters).

Fuglsang, P. & Madsen, H.A. 1999. Optimization method for wind turbine rotors. *Journal of Wind Engineering and Industrial Aerodynamics*, 80(1-2):191-206 doi:10.1016/S0167-6105(98)00191-3

Gasch, R., Maurer, J. & Heilmann, C. 2012. Blade geometry according to Betz and Schmitz. (*In* Gasch, R. & Twele, J., *eds*. Wind power plants: fundamentals, design, construction and operation. 2nd ed. Berlin: Springer. p. 168-207).

Hau, E. 2013. Wind turbines: fundamentals, technologies, application, economics. 3rd ed. Berlin: Springer.

Hibbeler, R.C. 2013. Mechanics of materials. 9th ed. Boston, MA: Prentice Hall.

Hsiao, F, Bai, C & Chong, W. 2013. The Performance Test of Three Different Horisontal Axis Wind Turbine (HAWT) Blade Shapes Using Experimental and Numerical Methods. *Energies,* 6:2774-2803 doi:10.3390/en6062784

Hsu, M.-C., Akkerman, I. & Bazilevs, Y. 2014. Finite element simulation of wind turbine aerodynamics: validation study using NREL Phase VI experiment. *Wind Energy*, 17:461-481 doi:10.1002/we.1599

Ingram, G. 2011. Wind turbine blade analysis using the blade element momentum method. Durham: Durham University. https://community.dur.ac.uk/g.l.ingram/download/wind_turbine_design.pdf Date of access: 10 Nov. 2018.

Jureczko, M., Pawlak, M. & Mężyk, A. 2005. Optimisation of wind turbine blades. *Journal of Materials Processing Technology*, 167(2-3):463-471 doi:10.1016/j.jmatprotec.2005.06.055

Kan, T., Nguyen, T.-D., White, J.C., Malhan, R.K. & Mi, C.C. 2017. A new integration method for an electric vehicle wireless charging system using LCC compensation topology: analysis and design. *IEEE Transactions on Power Electronics*, 32(2):1638-1650 doi:10.1109/TPEL.2016.2552060

LEAP CFD Team. 2012. Tips & tricks: convergence and mesh independence study. *LEAP Computational Fluid Dynamics Blog*, 17 Jan. https://www.computationalfluiddynamics.com.au/convergence-and-mesh-independent-study/ Date of access: 10 Nov. 2018.

Mabille, E. 2014. Wind Atlas for South Africa (WASA): Western Cape and parts of Northern and Eastern Cape - Brief introduction to working with WASA Files. http://stel-apps.csir.co.za/wasa-data/docs/Beginners%20Guide%20to%20Microsacle%20Modelling%20using%20WAsP_v5.pdf Date of access: 10 Nov. 2018.

Manwell, J.F. & McGowan, J.G. 2009. Wind energy explained: theory, design, and application. 2nd ed. Hoboken, NJ: John Wiley.

Marrero, D., Hernández, P., Suárez, L., Pestana, D., Benítez, A., Martín, J., Rivero, S. & Calero, E. 2014. Rotational molding applied to the manufacturing of blades of small wind turbine. Paper presented at the 12th Biennial ASME Conference on Engineering Systems Design and Analysis, Copenhagen, Denmark, 25-27 Jun. https://www.asme.org/products/proceedings/2014-2014-12th-biennial-conference-systems-design Date of access: 10 Nov. 2018.

Mendez, P.F. 1999. Order of magnitude scaling of complex engineering problems, and its application to high productivity arc welding. Cambridge, MA: MIT. (Thesis - PhD).

MIT (Massachusetts Institute of Technology). 2007. XFOIL: Subsonic airfoil development system. https://web.mit.edu/drela/Public/web/xfoil/ Date of access: 10 Nov. 2018.

Mullen, C. 2018. A review of finite element analysis with respect to experimental results. Paper presented at the 16th LACCEI International Multi-Conference for Engineering, Education, and Technology, Lima, Peru, 19-21 Jul. http://www.laccei.org/LACCEI2018-Lima/track_SD.html Date of access: 10 Nov. 2018.

National Instruments. 2016. National Instruments products for wind turbine condition monitoring. http://www.ni.com/white-paper/7676/en/ Date of access: 26 Oct. 2016.

Panagiotopoulou, O., Hutchinson, J., Rayfield, E., Wilshin, S. & Shefelbine, S. 2012. What makes an accurate and reliable subject-specific finite element model? A case study of an elephant femur. *Journal of the Royal Society Interface*, 9:351-361 doi:10.1098/rsif.2014.0854

RAENG (Royal Academy of Engineering). 2014a. Forces on large steam turbine blades. https://www.raeng.org.uk/publications/other/22-blade-forces Date of access: 10 Nov. 2018.

RAENG (Royal Academy of Engineering). 2014b. Wind turbine power calculations. https://www.raeng.org.uk/publications/other/23-wind-turbine Date of access: 10 Nov. 2018.

REN21 (Renewable Energy Policy Network for the 21st Century). 2014. Renewables 2014: Global status report. http://www.ren21.net/Portals/0/documents/Resources/GSR/2014/GSR2014_full%20report_low%20res.pdf Date of access: 10 Nov. 2018.

Retief, A.J. 2015. 4kW wind turbine blade. Potchefstroom, South Africa: NWU.

REUK (UK Renewable Energy Website). 2018. Wind turbine tip speed ratio. http://www.reuk.co.uk/wordpress/wind/wind-turbine-tip-speed-ratio/ Date of access: 12 Nov. 2018.

Sami, S., Zai, B.A. & Khan, M.A. 2014. Dynamic analysis of a 5kW wind turbine blade with experimental validation. *Journal of Space Technology*, 4(1):82-87. http://www.ist.edu.pk/jst/previous-issues/july-2014

Sandia National Laboratories. 2003. Cost Study for Large Wind Turbine Blades: WindPACT Blade System Design Studies. Albuquerque, New Mexico. SAND REPORT

SAWS (South African Weather Service). 2016. Potchefstroom Wind Speed Readings 2010-2016. http://www.weathersa.co.za/ Date of access: 10 Nov. 2018.

Scholtz, L., Muluadzi, K., Kritzinger, K., Mabaso, M. & Forder, S. 2017. WWF 2017 report: renewable energy: facts and futures.

https://www.crses.sun.ac.za/files/research/publications/popular-media-and-policy-brief/WWF_Energy%20Facts%20and%20Futures_Final%20Version.pdf Date of access: 10 Nov. 2018.

Schubel, P.J. & Crossley, R.J. 2012. Wind turbine blade design. *Energies*, 5(9):3425-3449 doi:10.3390/en5093425

Sedaghat, A., Hassanzadeh, A., Jamali, J., Mostafaeipour, A. & Chen, W.-H. 2017. Determination of rated wind speed for maximum annual energy production. *Applied Energy*, 205:781-789 doi:10.1016/j.apenergy.2017.08.079

Shih-Yu, Y., Yuan-Kang, W., Huei-Jeng, L. & Wei-Jen, L. 2013. Integrated mechanical and electrical DFIG wind turbine model development. Paper presented at the 2013 IEEE Industry Applications Society Annual Meeting, 6-11 Oct. https://ieeexplore.ieee.org/stamp/stamp.jsp?arnumber=6682471 Date of access: 10 Nov. 2018.

Tarfaoui, M. & Shah, O.R. 2013. Spar shape optimization of a multi megawatts composite wind turbine blade: modal analysis. (*In* Attaf, B., *ed.* Recent advances in composite materials for wind turbine blades. Hong Kong: World Academic Publishing. p. 93-104).

Tenguria, N., Mittal, N.D. & Ahmed, S. 2010. Design and finite element analysis of horizontal axis wind turbine blade. *International Journal of Applied Engineering Research, Dindigul*, 1(3):500-507. www.ipublishing.co.in/jarvol1no12010/EIJAER2018.pdf

The Engineering Toolbox. 2018. Engineering ToolBox - resources, tools and basic information for engineering and design of technical applications! https://www.engineeringtoolbox.com/young-modulus-d_417.html Date of access: 2 Dec. 2017.

Tong, W. 2010. Wind power generation and wind turbine design. Southampton: WIT press.

Twele, J. & Gasch, R. 2002. Wind power plants: fundamentals, design, construction and operation. Berlin: Springer.

Visser, G. 2014. How accurate is FEA? *ESTEQ Engineering Solutions*, 21 Oct. https://esteq.co.za/2014/10/21/accurate-fea/ Date of access: 7 Jun.

WindPower Progam. 2018. Wind turbine power output variation with steady wind speed. http://www.wind-power-program.com/turbine_characteristics.htm Date of access: 10 Nov. 2018.

Wood, M.D.K., Sun, X., Mai, Y., Rispler, A.R. & Mai, Y.-W. 2007. The effect of stitch distribution on Mode I delamination toughness of stitched laminated composites – experimental

results and FEA simulation. *Composites Science and Technology*, 67(6):1058-1072 doi:10.1016/j.compscitech.2006.06.002

APPENDIX A: MS EXCEL MODEL

The following tables show the MS Excel Model which was used to parameterise, process, and produce the results for the design.

The following table designates the parameters used as input to the model. Cells in green designate the user input, and blue cells designate the design process's automatically generated results from said parameters.

Table 24: Model input parameters and boundaries

Input	Value	Chord Length [m]	Pitch Angle (θ) [deg]
Wind Speed (Actual) [m/s]	2.15	0.42	29.00
Rotor RPM	42.00	0.46	21.00
Rotor Max Radius [m]	2.40	0.49	18.00
Blade Number (B)	3	0.39	14.00
Air Density [kg/m^3]	1.225	0.32	12.00
Dynamic Viscosity (μ) [Ns/m^2]	0.00001831	0.27	9.00
Rotor [rad/s]	10.75	0.24	7.00
E_airfoil [GPa]	2.3	0.21	6.00
E_alu [GPa]	69	0.19	5.00
Yield_airfoil [MPa]	8.7	0.17	4.00
Yield_alu [MPa]	240		
Airfoil_density [kg/m^3]	650		
Alu_density [kg/m^3]	2830		
Hub radius [m]	0.2		
Airfoil Thickness [mm]	7.00		

Model Status
Converged

Power [W]
56.28

Rotor Tip Speed [m/s]	10.75
Tip Speed Ratio	5.000

Procedure
1. Set speed to 2.15 m/s
2. Adjust for correct TSR (chord length and pitch)
3. Set to 17.5 m/s
4. Check minimum SF>1.05

Table 25: Aerodynamic design MS Excel code

Chord Length	Pitch Angle (θ) [deg]	CL	CD	a	b	Radius [m]	V_0 [m/s]
0.29	29	=Linear_Interpolate($F$26:$AM$26,$F$28:$AM$28,Q12)	0.0301744223849985	0.186747667911215	0.14263461397966	=$C$4*0.1+Interface!C16	=$B$13+H12*$B$13
0.32	21	=Linear_Interpolate($F$26:$AM$26,$F$28:$AM$28,Q13)	0.0147509456419329	0.236065061905134	0.0528536256460685	=$C$4*0.2+Interface!C16	=$B$13+H13*$B$13
0.34	18	=Linear_Interpolate($F$26:$AM$26,$F$29:$AM$29,Q14)	0.0139675928809794	0.247889168363049	0.00535602875211911	=$C$4*0.3+Interface!C16	=$B$13+H14*$B$13
0.31	14	=Linear_Interpolate($F$26:$AM$26,$F$30:$AM$30,Q15)	0.0114148037766482	0.22616455401599	0.00873218035221489	=$C$4*0.4+Interface!C16	=$B$13+H15*$B$13
0.28	12	=Linear_Interpolate($F$26:$AM$26,$F$31:$AM$31,Q16)	0.0108656936255946	0.19871755911547	0.0134327207909454	=$C$4*0.5+Interface!C16	=$B$13+H16*$B$13
0.25	9	=Linear_Interpolate($F$26:$AM$26,$F$32:$AM$32,Q17)	0.0106666451165562	0.213373626474078	0.0136174786790213	=$C$4*0.6+Interface!C16	=$B$13+H17*$B$13
0.23	7	=Linear_Interpolate($F$26:$AM$26,$F$33:$AM$33,Q18)	0.0104086097110632	0.213382886220885	0.0135392455781679	=$C$4*0.7+Interface!C16	=$B$13+H18*$B$13
0.21	6	=Linear_Interpolate($F$26:$AM$26,$F$34:$AM$34,Q19)	0.0103522681198388	0.214916850269862	0.0131275686754167	=$C$4*0.8+Interface!C16	=$B$13+H19*$B$13
0.18	5	=Linear_Interpolate($F$26:$AM$26,$F$35:$AM$35,Q20)	0.0113184720050362	0.221418955131454	0.0117160686909758	=$C$4*0.9+Interface!C16	=$B$13+H20*$B$13
0.17	4	=Linear_Interpolate($F$26:$AM$26,$F$36:$AM$36,Q21)	0.0150999561519572	0.2172046530723	0.0102907347278091	=$C$4*1+Interface!C16	=$B$13+H21*$B$13

V_1 [m/s]	V_2 [m/s]	Angle of Attack	φ [deg]	φ [rad]	Re	Lift [N]	Drag [N]
=((K12^2)+(M12^2))^0.5	=($C$8*J12)-(I12*($C$8*J12))	= O12-E12	=DEGREES(P12)	=ATAN(K12/M12	=($C$6*L12*D12)/$C$7	=F12*0.5*$C$6*(L12^2)*D12*($J$13-$J$12)	=G12*0.5*$C$6*(L12^2)*D12*($J$13-$J$12)
=((K13^2)+(M13^2))^0.5	=($C$8*J13)-(I13*($C$8*J13))	= O13-E13	=DEGREES(P13)	=ATAN(K13/M13	=($C$6*L13*D13)/$C$7	=F13*0.5*$C$6*(L13^2)*D13*($J$13-$J$12)	=G13*0.5*$C$6*(L13^2)*D13*($J$13-$J$12)
=((K14^2)+(M14^2))^0.5	=($C$8*J14)-(I14*($C$8*J14))	= O14-E14	=DEGREES(P14)	=ATAN(K14/M14	=($C$6*L14*D14)/$C$7	=F14*0.5*$C$6*(L14^2)*D14*($J$13-$J$12)	=G14*0.5*$C$6*(L14^2)*D14*($J$13-$J$12)
=((K15^2)+(M15^2))^0.5	=($C$8*J15)-(I15*($C$8*J15))	= O15-E15	=DEGREES(P15)	=ATAN(K15/M15	=($C$6*L15*D15)/$C$7	=F15*0.5*$C$6*(L15^2)*D15*($J$13-$J$12)	=G15*0.5*$C$6*(L15^2)*D15*($J$13-$J$12)
=((K16^2)+(M16^2))^0.5	=($C$8*J16)-(I16*($C$8*J16))	= O16-E16	=DEGREES(P16)	=ATAN(K16/M16	=($C$6*L16*D16)/$C$7	=F16*0.5*$C$6*(L16^2)*D16*($J$13-$J$12)	=G16*0.5*$C$6*(L16^2)*D16*($J$13-$J$12)
=((K17^2)+(M17^2))^0.5	=($C$8*J17)-(I17*($C$8*J17))	= O17-E17	=DEGREES(P17)	=ATAN(K17/M17	=($C$6*L17*D17)/$C$7	=F17*0.5*$C$6*(L17^2)*D17*($J$13-$J$12)	=G17*0.5*$C$6*(L17^2)*D17*($J$13-$J$12)
=((K18^2)+(M18^2))^0.5	=($C$8*J18)-(I18*($C$8*J18))	= O18-E18	=DEGREES(P18)	=ATAN(K18/M18	=($C$6*L18*D18)/$C$7	=F18*0.5*$C$6*(L18^2)*D18*($J$13-$J$12)	=G18*0.5*$C$6*(L18^2)*D18*($J$13-$J$12)
=((K19^2)+(M19^2))^0.5	=($C$8*J19)-(I19*($C$8*J19))	= O19-E19	=DEGREES(P19)	=ATAN(K19/M19	=($C$6*L19*D19)/$C$7	=F19*0.5*$C$6*(L19^2)*D19*($J$13-$J$12)	=G19*0.5*$C$6*(L19^2)*D19*($J$13-$J$12)
=((K20^2)+(M20^2))^0.5	=($C$8*J20)-(I20*($C$8*J20))	= O20-E20	=DEGREES(P20)	=ATAN(K20/M20	=($C$6*L20*D20)/$C$7	=F20*0.5*$C$6*(L20^2)*D20*($J$13-$J$12)	=G20*0.5*$C$6*(L20^2)*D20*($J$13-$J$12)
=((K21^2)+(M21^2))^0.5	=($C$8*J21)-(I21*($C$8*J21))	= O21-E21	=DEGREES(P21)	=ATAN(K21/M21	=($C$6*L21*D21)/$C$7	=F21*0.5*$C$6*(L21^2)*D21*($J$13-$J$12)	=G21*0.5*$C$6*(L21^2)*D21*($J$13-$J$12)

F_res [N]	F_res Direction β [deg]	F_res Adjustment β_2	Angle to adjust [deg]	Torque A	Thrust A
=SQRT(((R12)^2)+((S12)^2))	=DEGREES(ATAN(R12/S12))	=90-U12	=U12+N12-90	=(0.5*$C$6*(L12^2)*D12*((F12*SIN(AG12))+(G12*COS(AG12)))*$C$5*J12*($J$13-$J$12))	=(0.5*$C$6*(L12^2)*D12*((F12*COS(AG12))-(G12*SIN(AG12)))*$C$5*($J$13-$J$12))
=SQRT(((R13)^2)+((S13)^2))	=DEGREES(ATAN(R13/S13))	=90-U13	=U13+N13-90	=(0.5*$C$6*(L13^2)*D13*((F13*SIN(AG13))+(G13*COS(AG13)))*$C$5*J13*($J$13-$J$12))	=(0.5*$C$6*(L13^2)*D13*((F13*COS(AG13))-(G13*SIN(AG13)))*$C$5*($J$13-$J$12))
=SQRT(((R14)^2)+((S14)^2))	=DEGREES(ATAN(R14/S14))	=90-U14	=U14+N14-90	=(0.5*$C$6*(L14^2)*D14*((F14*SIN(AG14))+(G14*COS(AG14)))*$C$5*J14*($J$13-$J$12))	=(0.5*$C$6*(L14^2)*D14*((F14*COS(AG14))-(G14*SIN(AG14)))*$C$5*($J$13-$J$12))
=SQRT(((R15)^2)+((S15)^2))	=DEGREES(ATAN(R15/S15))	=90-U15	=U15+N15-90	=(0.5*$C$6*(L15^2)*D15*((F15*SIN(AG15))+(G15*COS(AG15)))*$C$5*J15*($J$13-$J$12))	=(0.5*$C$6*(L15^2)*D15*((F15*COS(AG15))-(G15*SIN(AG15)))*$C$5*($J$13-$J$12))
=SQRT(((R16)^2)+((S16)^2))	=DEGREES(ATAN(R16/S16))	=90-U16	=U16+N16-90	=(0.5*$C$6*(L16^2)*D16*((F16*SIN(AG16))+(G16*COS(AG16)))*$C$5*J16*($J$13-$J$12))	=(0.5*$C$6*(L16^2)*D16*((F16*COS(AG16))-(G16*SIN(AG16)))*$C$5*($J$13-$J$12))
=SQRT(((R17)^2)+((S17)^2))	=DEGREES(ATAN(R17/S17))	=90-U17	=U17+N17-90	=(0.5*$C$6*(L17^2)*D17*((F17*SIN(AG17))+(G17*COS(AG17)))*$C$5*J17*($J$13-$J$12))	=(0.5*$C$6*(L17^2)*D17*((F17*COS(AG17))-(G17*SIN(AG17)))*$C$5*($J$13-$J$12))
=SQRT(((R18)^2)+((S18)^2))	=DEGREES(ATAN(R18/S18))	=90-U18	=U18+N18-90	=(0.5*$C$6*(L18^2)*D18*((F18*SIN(AG18))+(G18*COS(AG18)))*$C$5*J18*($J$13-$J$12))	=(0.5*$C$6*(L18^2)*D18*((F18*COS(AG18))-(G18*SIN(AG18)))*$C$5*($J$13-$J$12))
=SQRT(((R19)^2)+((S19)^2))	=DEGREES(ATAN(R19/S19))	=90-U19	=U19+N19-90	=(0.5*$C$6*(L19^2)*D19*((F19*SIN(AG19))+(G19*COS(AG19)))*$C$5*J19*($J$13-$J$12))	=(0.5*$C$6*(L19^2)*D19*((F19*COS(AG19))-(G19*SIN(AG19)))*$C$5*($J$13-$J$12))
=SQRT(((R20)^2)+((S20)^2))	=DEGREES(ATAN(R20/S20))	=90-U20	=U20+N20-90	=(0.5*$C$6*(L20^2)*D20*((F20*SIN(AG20))+(G20*COS(AG20)))*$C$5*J20*($J$13-$J$12))	=(0.5*$C$6*(L20^2)*D20*((F20*COS(AG20))-(G20*SIN(AG20)))*$C$5*($J$13-$J$12))
=SQRT(((R21)^2)+((S21)^2))	=DEGREES(ATAN(R21/S21))	=90-U21	=U21+N21-90	=(0.5*$C$6*(L21^2)*D21*((F21*SIN(AG21))+(G21*COS(AG21)))*$C$5*J21*($J$13-$J$12))	=(0.5*$C$6*(L21^2)*D21*((F21*COS(AG21))-(G21*SIN(AG21)))*$C$5*($J$13-$J$12))
				=SUM(Y12:Y21)	=SUM(Z12:Z21)
				=$Y$22*$C$8	Power [W]

Torque B	Thrust B	Torque error [%]	Thrust error [%]	Total error [%]
=4*$C$6*PI()*(J12^3)*$B$13*(1+H12)*I12*$C$8*($J$13-$J$12)	=4*$C$6*PI()*J12*($B$13^2)*(1+H12)*H12*($J$13-$J$12)	=((Y12-AA12)*100)/Y12	=((AB12-Z12)*100)/Z12	=AC12+AD12
=4*$C$6*PI()*(J13^3)*$B$13*(1+H13)*I13*$C$8*($J$13-$J$12)	=4*$C$6*PI()*J13*($B$13^2)*(1+H13)*H13*($J$13-$J$12)	=((Y13-AA13)*100)/Y13	=((AB13-Z13)*100)/Z13	=AC13+AD13
=4*$C$6*PI()*(J14^3)*$B$13*(1+H14)*I14*$C$8*($J$13-$J$12)	=4*$C$6*PI()*J14*($B$13^2)*(1+H14)*H14*($J$13-$J$12)	=((Y14-AA14)*100)/Y14	=((AB14-Z14)*100)/Z14	=AC14+AD14
=4*$C$6*PI()*(J15^3)*$B$13*(1+H15)*I15*$C$8*($J$13-$J$12)	=4*$C$6*PI()*J15*($B$13^2)*(1+H15)*H15*($J$13-$J$12)	=((Y15-AA15)*100)/Y15	=((AB15-Z15)*100)/Z15	=AC15+AD15
=4*$C$6*PI()*(J16^3)*$B$13*(1+H16)*I16*$C$8*($J$13-$J$12)	=4*$C$6*PI()*J16*($B$13^2)*(1+H16)*H16*($J$13-$J$12)	=((Y16-AA16)*100)/Y16	=((AB16-Z16)*100)/Z16	=AC16+AD16
=4*$C$6*PI()*(J17^3)*$B$13*(1+H17)*I17*$C$8*($J$13-$J$12)	=4*$C$6*PI()*J17*($B$13^2)*(1+H17)*H17*($J$13-$J$12)	=((Y17-AA17)*100)/Y17	=((AB17-Z17)*100)/Z17	=AC17+AD17
=4*$C$6*PI()*(J18^3)*$B$13*(1+H18)*I18*$C$8*($J$13-$J$12)	=4*$C$6*PI()*J18*($B$13^2)*(1+H18)*H18*($J$13-$J$12)	=((Y18-AA18)*100)/Y18	=((AB18-Z18)*100)/Z18	=AC18+AD18
=4*$C$6*PI()*(J19^3)*$B$13*(1+H19)*I19*$C$8*($J$13-$J$12)	=4*$C$6*PI()*J19*($B$13^2)*(1+H19)*H19*($J$13-$J$12)	=((Y19-AA19)*100)/Y19	=((AB19-Z19)*100)/Z19	=AC19+AD19
=4*$C$6*PI()*(J20^3)*$B$13*(1+H20)*I20*$C$8*($J$13-$J$12)	=4*$C$6*PI()*J20*($B$13^2)*(1+H20)*H20*($J$13-$J$12)	=((Y20-AA20)*100)/Y20	=((AB20-Z20)*100)/Z20	=AC20+AD20
=4*$C$6*PI()*(J21^3)*$B$13*(1+H21)*I21*$C$8*($J$13-$J$12)	=4*$C$6*PI()*J21*($B$13^2)*(1+H21)*H21*($J$13-$J$12)	=((Y21-AA21)*100)/Y21	=((AB21-Z21)*100)/Z21	=AC21+AD21
=SUM(AA12:AA21)	=SUM(AB12:AB21)	=SUM(AC12:AC21)	=SUM(AD12:AD21)	=SUM(AE12:AE21)
=$AA$22*$C$8	Power [W]			

Blades	=Interface!C6							
Section Tip Speed	**[m/s]**	**Tip Speed ratio**	**[-]**	**Relative flow angle**	**[rad]**		**Radius**	**[m]**
v_1	=I4*'Aero Model'!$C$8	λ_r_1	=C4/'Aero Model'!$C$2	Beta_1	=(PI()/2)-((2/3)*(ATAN(1/E4)))		r_1	='Aero Model'!J12
v_2	=I5*'Aero Model'!$C$8	λ_r_2	=C5/'Aero Model'!$C$2	Beta_2	=(PI()/2)-((2/3)*(ATAN(1/E5)))		r_2	='Aero Model'!J13
v_3	=I6*'Aero Model'!$C$8	λ_r_3	=C6/'Aero Model'!$C$2	Beta_3	=(PI()/2)-((2/3)*(ATAN(1/E6)))		r_3	='Aero Model'!J14
v_4	=I7*'Aero Model'!$C$8	λ_r_4	=C7/'Aero Model'!$C$2	Beta_4	=(PI()/2)-((2/3)*(ATAN(1/E7)))		r_4	='Aero Model'!J15
v_5	=I8*'Aero Model'!$C$8	λ_r_5	=C8/'Aero Model'!$C$2	Beta_5	=(PI()/2)-((2/3)*(ATAN(1/E8)))		r_5	='Aero Model'!J16
v_6	=I9*'Aero Model'!$C$8	λ_r_6	=C9/'Aero Model'!$C$2	Beta_6	=(PI()/2)-((2/3)*(ATAN(1/E9)))		r_6	='Aero Model'!J17
v_7	=I10*'Aero Model'!$C$8	λ_r_7	=C10/'Aero Model'!$C$2	Beta_7	=(PI()/2)-((2/3)*(ATAN(1/E10)))		r_7	='Aero Model'!J18
v_8	=I11*'Aero Model'!$C$8	λ_r_8	=C11/'Aero Model'!$C$2	Beta_8	=(PI()/2)-((2/3)*(ATAN(1/E11)))		r_8	='Aero Model'!J19
v_9	=I12*'Aero Model'!$C$8	λ_r_9	=C12/'Aero Model'!$C$2	Beta_9	=(PI()/2)-((2/3)*(ATAN(1/E12)))		r_9	='Aero Model'!J20
v_10	=I13*'Aero Model'!$C$8	λ_r_10	=C13/'Aero Model'!$C$2	Beta_10	=(PI()/2)-((2/3)*(ATAN(1/E13)))		r_10	='Aero Model'!J21
Chord Length	**[m]**							
c_1	=(8*(PI()))*I4*(COS(G4)))/(3*$C$2*E4)							
c_2	=(8*(PI()))*I5*(COS(G5)))/(3*$C$2*E5)							
c_3	=(8*(PI()))*I6*(COS(G6)))/(3*$C$2*E6)							
c_4	=(8*(PI()))*I7*(COS(G7)))/(3*$C$2*E7)							
c_5	=(8*(PI()))*I8*(COS(G8)))/(3*$C$2*E8)							
c_6	=(8*(PI()))*I9*(COS(G9)))/(3*$C$2*E9)							
c_7	=(8*(PI()))*I10*(COS(G10)))/(3*$C$2*E10)							
c_8	=(8*(PI()))*I11*(COS(G11)))/(3*$C$2*E11)							
c_9	=(8*(PI()))*I12*(COS(G12)))/(3*$C$2*E12)							
c_10	=(8*(PI()))*I13*(COS(G13)))/(3*$C$2*E13)							

Note that the raw data used in this analysis is not included, as it contains hourly wind speed data over the course of multiple years and consists of more than 150 000 individual data points. The following equations are applicable to any of the years' data and equations per year are omitted to avoid redundancy.

Table 26: Finding the optimum design wind speed for Potchefstroom region

Calculate Bin count According to Rice's Rule							
=2*(8500^(1/3))							
40							
Year	**2011**	**2012**	**2013**	**2014**	**2015**	**2016**	
Max Wind Speed [m/s]	=MAX(K2:K8377)	=MAX(W2:W8713)	=MAX(AI2:AI8447)	=MAX(AU2:AU8468)	=MAX(BG2:BG8663)	=MAX(BS2:BS8593)	
Average Wind Speed [m/s]	=S3	=AE3	=AQ3	=BC3	=BO3	=CA3	
Average Power per Area	=AVERAGE(S5,AE5,BO5,CA5)	[W/m^2]					
Wind Speeds [m/s]	**2011**	**2012**	**2013**	**2014**	**2015**	**2016**	
0-2	0.4119	=SUM(AA2:AA9)	=SUM(AM2:AM9)	=SUM(AY2:AY9)	=SUM(BK2:BK9)	=SUM(BW2:BW9)	**=AVERAGE(B9:G9)**
2-4	=SUM(O10:O17)	=SUM(AA10:AA17)	=SUM(AM10:AM17)	=SUM(AY10:AY17)	=SUM(BK10:BK17)	=SUM(BW10:BW17)	=AVERAGE(B10:G10)
4-6	=SUM(O18:O25)	=SUM(AA18:AA25)	=SUM(AM18:AM25)	=SUM(AY18:AY25)	=SUM(BK18:BK25)	=SUM(BW18:BW25)	=AVERAGE(B11:G11)
6-8	=SUM(O26:O33)	=SUM(AA26:AA33)	=SUM(AM26:AM33)	=SUM(AY26:AY33)	=SUM(BK26:BK33)	=SUM(BW26:BW33)	=AVERAGE(B12:G12)
8-10	=SUM(O34:O41)	=SUM(AA34:AA41)	=SUM(AM34:AM41)	=SUM(AY34:AY41)	=SUM(BK34:BK41)	=SUM(BW34:BW41)	=AVERAGE(B13:G13)
10-11.25	=SUM(O42:O47)	=SUM(AA42:AA47)	=SUM(AM42:AM47)	=SUM(AY42:AY47)	=SUM(BK42:BK47)	=SUM(BW42:BW47)	=AVERAGE(B14:G14)
	=SUM(B9:B14)	=SUM(C9:C14)	=SUM(D9:D14)	=SUM(E9:E14)	=SUM(F9:F14)	=SUM(G9:G14)	=SUM(H9:H14)
Therfore							
0-6 [m/s]	=SUM(B9:B11)	=SUM(C9:C11)	=SUM(D9:D11)	=SUM(E9:E11)	=SUM(F9:F11)	=SUM(G9:G11)	=AVERAGE(B17:G17)
6-12 [m/s]	=SUM(B12:B14)	=SUM(C12:C14)	=SUM(D12:D14)	=SUM(E12:E14)	=SUM(F12:F14)	=SUM(G12:G14)	=AVERAGE(B18:G18)
							=SUM(H12:H14)

k	28.6509299869309	Shape Factor
u_bar	=AVERAGE(K2:K8377)	Ave Wind Speed [m/s]
lambda (c)	=S3/(EXP(GAMMALN(1+(1/S2))))	Scale Factor
Data Power Ave	=L8378	[W/m^2]
Weibull Power Ave	=Q48	[W/m^2]

Bins	Frequency	% of Time	Weibull	Wind Power Weibull [W/m^2]
0	=FREQUENCY(K2:K8377,M2:M47)	=N2/8276	=WEIBULL.DIST(M2,$S$2,$S$4,FALSE)	=0.5*Interface!$C$7*(M2^3)*P2
0.25	=FREQUENCY(K2:K8377,M2:M47)	=N3/8276	=WEIBULL.DIST(M3,$S$2,$S$4,FALSE)	=0.5*Interface!$C$7*(M3^3)*P3
0.5	=FREQUENCY(K2:K8377,M2:M47)	=N4/8276	=WEIBULL.DIST(M4,$S$2,$S$4,FALSE)	=0.5*Interface!$C$7*(M4^3)*P4
0.75	=FREQUENCY(K2:K8377,M2:M47)	=N5/8276	=WEIBULL.DIST(M5,$S$2,$S$4,FALSE)	=0.5*Interface!$C$7*(M5^3)*P5
1	=FREQUENCY(K2:K8377,M2:M47)	=N6/8276	=WEIBULL.DIST(M6,$S$2,$S$4,FALSE)	=0.5*Interface!$C$7*(M6^3)*P6
1.25	=FREQUENCY(K2:K8377,M2:M47)	=N7/8276	=WEIBULL.DIST(M7,$S$2,$S$4,FALSE)	=0.5*Interface!$C$7*(M7^3)*P7
1.5	=FREQUENCY(K2:K8377,M2:M47)	=N8/8276	=WEIBULL.DIST(M8,$S$2,$S$4,FALSE)	=0.5*Interface!$C$7*(M8^3)*P8
1.75	=FREQUENCY(K2:K8377,M2:M47)	=N9/8276	=WEIBULL.DIST(M9,$S$2,$S$4,FALSE)	=0.5*Interface!$C$7*(M9^3)*P9
2	=FREQUENCY(K2:K8377,M2:M47)	=N10/8276	=WEIBULL.DIST(M10,$S$2,$S$4,FALSE)	=0.5*Interface!$C$7*(M10^3)*P10
2.25	=FREQUENCY(K2:K8377,M2:M47)	=N11/8276	=WEIBULL.DIST(M11,$S$2,$S$4,FALSE)	=0.5*Interface!$C$7*(M11^3)*P11
2.5	=FREQUENCY(K2:K8377,M2:M47)	=N12/8276	=WEIBULL.DIST(M12,$S$2,$S$4,FALSE)	=0.5*Interface!$C$7*(M12^3)*P12
2.75	=FREQUENCY(K2:K8377,M2:M47)	=N13/8276	=WEIBULL.DIST(M13,$S$2,$S$4,FALSE)	=0.5*Interface!$C$7*(M13^3)*P13
3	=FREQUENCY(K2:K8377,M2:M47)	=N14/8276	=WEIBULL.DIST(M14,$S$2,$S$4,FALSE)	=0.5*Interface!$C$7*(M14^3)*P14
3.25	=FREQUENCY(K2:K8377,M2:M47)	=N15/8276	=WEIBULL.DIST(M15,$S$2,$S$4,FALSE)	=0.5*Interface!$C$7*(M15^3)*P15
3.5	=FREQUENCY(K2:K8377,M2:M47)	=N16/8276	=WEIBULL.DIST(M16,$S$2,$S$4,FALSE)	=0.5*Interface!$C$7*(M16^3)*P16
3.75	=FREQUENCY(K2:K8377,M2:M47)	=N17/8276	=WEIBULL.DIST(M17,$S$2,$S$4,FALSE)	=0.5*Interface!$C$7*(M17^3)*P17
4	=FREQUENCY(K2:K8377,M2:M47)	=N18/8276	=WEIBULL.DIST(M18,$S$2,$S$4,FALSE)	=0.5*Interface!$C$7*(M18^3)*P18
4.25	=FREQUENCY(K2:K8377,M2:M47)	=N19/8276	=WEIBULL.DIST(M19,$S$2,$S$4,FALSE)	=0.5*Interface!$C$7*(M19^3)*P19
4.5	=FREQUENCY(K2:K8377,M2:M47)	=N20/8276	=WEIBULL.DIST(M20,$S$2,$S$4,FALSE)	=0.5*Interface!$C$7*(M20^3)*P20
4.75	=FREQUENCY(K2:K8377,M2:M47)	=N21/8276	=WEIBULL.DIST(M21,$S$2,$S$4,FALSE)	=0.5*Interface!$C$7*(M21^3)*P21
5	=FREQUENCY(K2:K8377,M2:M47)	=N22/8276	=WEIBULL.DIST(M22,$S$2,$S$4,FALSE)	=0.5*Interface!$C$7*(M22^3)*P22
5.25	=FREQUENCY(K2:K8377,M2:M47)	=N23/8276	=WEIBULL.DIST(M23,$S$2,$S$4,FALSE)	=0.5*Interface!$C$7*(M23^3)*P23
5.5	=FREQUENCY(K2:K8377,M2:M47)	=N24/8276	=WEIBULL.DIST(M24,$S$2,$S$4,FALSE)	=0.5*Interface!$C$7*(M24^3)*P24
5.75	=FREQUENCY(K2:K8377,M2:M47)	=N25/8276	=WEIBULL.DIST(M25,$S$2,$S$4,FALSE)	=0.5*Interface!$C$7*(M25^3)*P25
6	=FREQUENCY(K2:K8377,M2:M47)	=N26/8276	=WEIBULL.DIST(M26,$S$2,$S$4,FALSE)	=0.5*Interface!$C$7*(M26^3)*P26
6.25	=FREQUENCY(K2:K8377,M2:M47)	=N27/8276	=WEIBULL.DIST(M27,$S$2,$S$4,FALSE)	=0.5*Interface!$C$7*(M27^3)*P27
6.5	=FREQUENCY(K2:K8377,M2:M47)	=N28/8276	=WEIBULL.DIST(M28,$S$2,$S$4,FALSE)	=0.5*Interface!$C$7*(M28^3)*P28
6.75	=FREQUENCY(K2:K8377,M2:M47)	=N29/8276	=WEIBULL.DIST(M29,$S$2,$S$4,FALSE)	=0.5*Interface!$C$7*(M29^3)*P29
7	=FREQUENCY(K2:K8377,M2:M47)	=N30/8276	=WEIBULL.DIST(M30,$S$2,$S$4,FALSE)	=0.5*Interface!$C$7*(M30^3)*P30
7.25	=FREQUENCY(K2:K8377,M2:M47)	=N31/8276	=WEIBULL.DIST(M31,$S$2,$S$4,FALSE)	=0.5*Interface!$C$7*(M31^3)*P31
7.5	=FREQUENCY(K2:K8377,M2:M47)	=N32/8276	=WEIBULL.DIST(M32,$S$2,$S$4,FALSE)	=0.5*Interface!$C$7*(M32^3)*P32
7.75	=FREQUENCY(K2:K8377,M2:M47)	=N33/8276	=WEIBULL.DIST(M33,$S$2,$S$4,FALSE)	=0.5*Interface!$C$7*(M33^3)*P33
8	=FREQUENCY(K2:K8377,M2:M47)	=N34/8276	=WEIBULL.DIST(M34,$S$2,$S$4,FALSE)	=0.5*Interface!$C$7*(M34^3)*P34
8.25	=FREQUENCY(K2:K8377,M2:M47)	=N35/8276	=WEIBULL.DIST(M35,$S$2,$S$4,FALSE)	=0.5*Interface!$C$7*(M35^3)*P35
8.5	=FREQUENCY(K2:K8377,M2:M47)	=N36/8276	=WEIBULL.DIST(M36,$S$2,$S$4,FALSE)	=0.5*Interface!$C$7*(M36^3)*P36
8.75	=FREQUENCY(K2:K8377,M2:M47)	=N37/8276	=WEIBULL.DIST(M37,$S$2,$S$4,FALSE)	=0.5*Interface!$C$7*(M37^3)*P37
9	=FREQUENCY(K2:K8377,M2:M47)	=N38/8276	=WEIBULL.DIST(M38,$S$2,$S$4,FALSE)	=0.5*Interface!$C$7*(M38^3)*P38
9.25	=FREQUENCY(K2:K8377,M2:M47)	=N39/8276	=WEIBULL.DIST(M39,$S$2,$S$4,FALSE)	=0.5*Interface!$C$7*(M39^3)*P39
9.5	=FREQUENCY(K2:K8377,M2:M47)	=N40/8276	=WEIBULL.DIST(M40,$S$2,$S$4,FALSE)	=0.5*Interface!$C$7*(M40^3)*P40
9.75	=FREQUENCY(K2:K8377,M2:M47)	=N41/8276	=WEIBULL.DIST(M41,$S$2,$S$4,FALSE)	=0.5*Interface!$C$7*(M41^3)*P41
10	=FREQUENCY(K2:K8377,M2:M47)	=N42/8276	=WEIBULL.DIST(M42,$S$2,$S$4,FALSE)	=0.5*Interface!$C$7*(M42^3)*P42
10.25	=FREQUENCY(K2:K8377,M2:M47)	=N43/8276	=WEIBULL.DIST(M43,$S$2,$S$4,FALSE)	=0.5*Interface!$C$7*(M43^3)*P43
10.5	=FREQUENCY(K2:K8377,M2:M47)	=N44/8276	=WEIBULL.DIST(M44,$S$2,$S$4,FALSE)	=0.5*Interface!$C$7*(M44^3)*P44
10.75	=FREQUENCY(K2:K8377,M2:M47)	=N45/8276	=WEIBULL.DIST(M45,$S$2,$S$4,FALSE)	=0.5*Interface!$C$7*(M45^3)*P45
11	=FREQUENCY(K2:K8377,M2:M47)	=N46/8276	=WEIBULL.DIST(M46,$S$2,$S$4,FALSE)	=0.5*Interface!$C$7*(M46^3)*P46
11.25	=FREQUENCY(K2:K8377,M2:M47)	=N47/8276	=WEIBULL.DIST(M47,$S$2,$S$4,FALSE)	=0.5*Interface!$C$7*(M47^3)*P47
			Sum Weibll Pwr	=SUM(Q2:Q47)

Table 27: Structural design Excel code

Structural Input		
Air Density	='Aero Model'!C6	[kg/m^3]
Wind Speed	='Aero Model'!B13	[m/s]
Dynamic Wind Pressure	=0.5*$S$4*($S$5^2)	[Pa]
Shell Thickness	='Airfoil Inertia'!B1	mm
E_airfoil	=Interface!C10	GPa
E_alu	=Interface!C11	Gpa
Yield_airfoil	=Interface!C12	Mpa
Yield_alu	=Interface!C13	MPa

Section 1		
Cross Sectional Area (A)	='Airfoil Inertia'!L206	[m^2]
Width_1	='Aero Model'!D12	[m]
Length_1	=$AG$9/10	[m]
Area	=S15*S16	[m^2]
F_directwind_1	*=$S$6*S17*	*[N]*
MidpointShear_1	=V5-(Z3*U15)	[N]
MidpointMoment_1	=V5*U15-V6-(Z3*((U15^2)/2))	[N.m.]
Section 2		
Cross Sectional Area (A)	='Airfoil Inertia'!AC206	[m^2]
Width_2	='Aero Model'!D13	[m]
Length_2	=$AG$9/10	[m]
Area_2	=S23*S24	[m^2]
F_directwind_2	*=$S$6*S25*	*[N]*
MidpointShear_2	=V5-(Z3*S16)-(Z4*(U17-S16))	[N]
MidpointMoment_2	=V5*U17-V6-((Z3*S16)*((U17-V17)+((W15-V15)/2)))-(Z4*(((U17-V17)^2)/2))	[N.m.]
Section 3		
Cross Sectional Area (A)	='Airfoil Inertia'!AU206	[m^2]
Width_3	='Aero Model'!D14	[m]
Length_3	=$AG$9/10	[m]
Area_3	=S31*S32	[m^2]
F_directwind_3	*=$S$6*S33*	*[N]*
MidpointShear_3	=V5-(Z3*S16)-(Z4*S24)-(Z5*(U19-V19))	[N]
MidpointMoment_3	=V5*U19-V6-(Z3*(W15-V15)*((U19-W15)+((W17-V17)/2)))-(Z4*(W17-V17)*((U19-V19	[N.m.]
Section 4		
Cross Sectional Area (A)	='Airfoil Inertia'!BM206	[m^2]
Width_4	='Aero Model'!D15	[m]
Length_4	=$AG$9/10	[m]
Area_4	=S39*S40	[m^2]
F_directwind_4	*=$S$6*S41*	*[N]*
MidpointShear_4	=V5-(Z3*S16)-(Z4*S24)-(Z5*S32)-(Z6*(U21-V21))	[N]
MidpointMoment_4	=V5*U21-V6-Z3*(W15-V15)*((U21-W15)+((W15-V15)/2))-Z4*(W17-V17)*((U21-V19)+	[N.m.]
Section 5		
Cross Sectional Area (A)	='Airfoil Inertia'!CE206	[m^2]
Width_5	='Aero Model'!D16	[m]
Length_5	=$AG$9/10	[m]
Area_5	=S47*S48	[m^2]
F_directwind_5	*=$S$6*S49*	*[N]*
MidpointShear_5	=V5-(Z3*S16)-(Z4*S24)-(Z5*S32)-(Z6*S40)-(Z7*(U23-V23))	[N]
MidpointMoment_5	=V5*U23-V6-Z3*(W15-V15)*((U23-W15)+((W15-V15)/2))-Z4*(W17-V17)*((U23-W17)+	[N.m.]

Section 6		
Cross Sectional Area (A)	='Airfoil Inertia'!CX206	[m^2]
Width_6	='Aero Model'!D17	[m]
Length_6	=$AG$9/10	[m]
Area_6	=S55*S56	[m^2]
F_directwind_6	*=$$$6*S57*	*[N]*
MidpointShear_6	=V5-(Z3*S16)-(Z4*S24)-(Z5*S32)-(Z6*S40)-(Z7*S48)-(Z8*(U25-V25))	[N]
MidpointMoment_6	=V5*U25-V6-Z3*(W15-V15)*((U25-W15)+((W15-V15)/2))-Z4*(W17-V17)*((U25-W17)+((W17-V17)/2))-Z5*(W19-V19)*((U25-W19)+((W19-V19)/2))-Z6*(W21-V21)*((U25-W21)+((W21-V21)/2))-Z7*(W23-V23)*((U25-W23)+((W2	[N.m.]
Section 7		
Cross Sectional Area (A)	='Airfoil Inertia'!DP206	[m^2]
Width_7	='Aero Model'!D18	[m]
Length_7	=$AG$9/10	[m]
Area_7	=S63*S64	[m^2]
F_directwind_7	*=$$$6*S65*	*[N]*
MidpointShear_7	=V5-(Z3*S16)-(Z4*S24)-(Z5*S32)-(Z6*S40)-(Z7*S48)-(Z8*S56)-(Z9*(U27-V27))	[N]
MidpointMoment_7	=V5*U27-V6-Z3*(W15-V15)*((U27-W15)+((W15-V15)/2))-Z4*(W17-V17)*((U27-W17)+((W17-V17)/2))-Z5*(W19-V19)*((U27-W19)+((W19-V19)/2))-Z6*(W21-V21)*((U27-W21)+((W21-V21)/2))-Z7*(W23-V23)*((U27-W23)+((W2	[N.m.]
Section 8		
Cross Sectional Area (A)	='Airfoil Inertia'!EH206	[m^2]
Width_8	='Aero Model'!D19	[m]
Length_8	=$AG$9/10	[m]
Area_8	=S71*S72	[m^2]
F_directwind_8	*=$$$6*S73*	*[N]*
MidpointShear_8	=V5-(Z3*S16)-(Z4*S24)-(Z5*S32)-(Z6*S40)-(Z7*S48)-(Z8*S56)-(Z9*S64)-(Z10*(U29-V29))	[N]
MidpointMoment_8	=V5*U29-V6-Z3*(W15-V15)*((U29-W15)+((W15-V15)/2))-Z4*(W17-V17)*((U29-W17)+((W17-V17)/2))-Z5*(W19-V19)*((U29-W19)+((W19-V19)/2))-Z6*(W21-V21)*((U29-W21)+((W21-V21)/2))-Z7*(W23-V23)*((U29-W23)+((W2	[N.m.]
Section 9		
Cross Sectional Area (A)	='Airfoil Inertia'!EZ206	[m^2]
Width_9	='Aero Model'!D20	[m]
Length_9	=$AG$9/10	[m]
Area_9	=S79*S80	[m^2]
F_directwind_9	*=$$$6*S81*	*[N]*
MidpointShear_9	=V5-(Z3*S16)-(Z4*S24)-(Z5*S32)-(Z6*S40)-(Z7*S48)-(Z8*S56)-(Z9*S64)-(Z10*(S72))-(Z11*(U31-V31))	[N]
MidpointMoment_9	=V5*U31-V6-Z3*(W15-V15)*((U31-W15)+((W15-V15)/2))-Z4*(W17-V17)*((U31-W17)+((W17-V17)/2))-Z5*(W19-V19)*((U31-W19)+((W19-V19)/2))-Z6*(W21-V21)*((U31-W21)+((W21-V21)/2))-Z7*(W23-V23)*((U31-W23)+((W2	[N.m.]
Section 10		
Cross Sectional Area (A)	='Airfoil Inertia'!FR206	[m^2]
Width_10	='Aero Model'!D21	[m]
Length_10	=$AG$9/10	[m]
Area_10	=S87*S88	[m^2]
F_directwind_10	*=$$$6*S89*	*[N]*
MidpointShear_10	=V5-(Z3*S16)-(Z4*S24)-(Z5*S32)-(Z6*S40)-(Z7*S48)-(Z8*S56)-(Z9*S64)-(Z10*(S72))-(Z11*S80)-(Z12*(U33-V33))	[N]
MidpointMoment_10	=V5*U33-V6-Z3*(W15-V15)*((U33-W15)+((W15-V15)/2))-Z4*(W17-V17)*((U33-W17)+((W17-V17)/2))-Z5*(W19-V19)*((U33-W19)+((W19-V19)/2))-Z6*(W21-V21)*((U33-W21)+((W21-V21)/2))-Z7*(W23-V23)*((U33-W23)+((W2	[N.m.]

Shear due to Wind for each Section		
R_A	=Z3*S16+Z4*S24+Z5*S32+Z6*S40+Z7*S48+Z8*S56+Z9*S64+Z10*S72+Z11*S80+Z12*S88	[N]
M_A	=Z13+Z14+Z15+Z16+Z17+Z18+Z19+Z20+Z21+Z22	[N.m.]
x_1	L_0	L_1
=S16/2	=($AG$9/10)*0	=($AG$9/10)*1
x_2	L_1	L_2
=S16+(S24/2)	=($AG$9/10)*1	=($AG$9/10)*2
x_3	L_2	L_3
=(S16+S24+(S32/2))	=($AG$9/10)*2	=($AG$9/10)*3
x_4	L_3	L_4
=(S16+S24+S32+(S40/2))	=($AG$9/10)*3	=($AG$9/10)*4
x_5	L_4	L_5
=(S16+S24+S32+S40+(S48/2))	=($AG$9/10)*4	=($AG$9/10)*5
x_6	L_5	L_6
=(S16+S24+S32+S40+S48+(S56/2))	=($AG$9/10)*5	=($AG$9/10)*6
x_7	L_6	L_7
=(S16+S24+S32+S40+S48+S56+(S64/2))	=($AG$9/10)*6	=($AG$9/10)*7
8	L_7	L_8
=(S16+S24+S32+S40+S48+S56+S64+(S72/2))	=($AG$9/10)*7	=($AG$9/10)*8
x_9	L_8	L_9
=(S16+S24+S32+S40+S48+S56+S64+S72+(S80/2))	=($AG$9/10)*8	=($AG$9/10)*9
x_10	L_9	L_10
=(S16+S24+S32+S40+S48+S56+S64+S72+S80+(S88/2))	=($AG$9/10)*9	=($AG$9/10)*10

STRUCTURAL INPUT		
Airfoil material ρ	=Interface!C14	[kg/m^3]
Rotor RPM	='Aero Model'!C3	[RPM]
Rotor ω	=(AG5*2*PI())/60	[rad/s]
Hub Radius	=Interface!C16	[m]
Blde Root Area (A_root)	0.008	[m^2]
Blade Length	='Aero Model'!C4	[m]
Centrifugal Force (airfoil)		
Summed Force	=AG17+AG25+AG33+AG41+AG49+AG57+AG65+AG73+AG81+AG89	[N]
Root Stress	=AG11/AG8	[Pa]
Section 1		
Cross Sectional Area (A)	='Airfoil Inertia'!L206	[m^2]
r1	=($AG$9/10)*1+$AG$7	[m]
r0	=($AG$9/10)*0+$AG$7	[m]
F_1	=$AG$4*AG14*($AG$6^2)*(((AG15^2)-(AG16^2))/2)	[N]
F_sum1	=AG17+AG26	[N]
σ_1	=AG18/AG14	[Pa]
	=AG19/1000000	[Mpa]
Section 2		
Cross Sectional Area (A)	='Airfoil Inertia'!AC206	[m^2]
r2	=($AG$9/10)*2+$AG$7	[m]
r1	=($AG$9/10)*1+$AG$7	[m]
F_2	=$AG$4*AG22*($AG$6^2)*(((AG23^2)-(AG24^2))/2)	[N]
F_sum2	=AG25+AG34	[N]
σ_2	=AG26/AG22	[Pa]
	=AG27/1000000	[Mpa]
Section 3		
Cross Sectional Area (A)	='Airfoil Inertia'!AU206	[m^2]
r3	=($AG$9/10)*3+$AG$7	[m]
r2	=($AG$9/10)*2+$AG$7	[m]
F_3	=$AG$4*AG30*($AG$6^2)*(((AG31^2)-(AG32^2))/2)	[N]
F_sum3	=AG33+AG42	
σ_3	=AG34/AG30	[Pa]
	=AG35/1000000	[Mpa]
Section 4		
Cross Sectional Area (A)	='Airfoil Inertia'!BM206	[m^2]
r4	=($AG$9/10)*4+$AG$7	[m]
r3	=($AG$9/10)*3+$AG$7	[m]
F_4	=$AG$4*AG38*($AG$6^2)*(((AG39^2)-(AG40^2))/2)	[N]
F_sum4	=AG41+AG50	
σ_4	=AG42/AG38	[Pa]
	=AG43/1000000	[Mpa]
Section 5		
Cross Sectional Area (A)	='Airfoil Inertia'!CE206	[m^2]
r5	=($AG$9/10)*5+$AG$7	[m]
r4	=($AG$9/10)*4+$AG$7	[m]
F_5	=$AG$4*AG46*($AG$6^2)*(((AG47^2)-(AG48^2))/2)	[N]
F_sum5	=AG49+AG58	
σ_5	=AG50/AG46	[Pa]
	=AG51/1000000	[Mpa]
Section 6		
Cross Sectional Area (A)	='Airfoil Inertia'!CX206	[m^2]
r6	=($AG$9/10)*6+$AG$7	[m]
r5	=($AG$9/10)*5+$AG$7	[m]
F_6	=$AG$4*AG54*($AG$6^2)*(((AG55^2)-(AG56^2))/2)	[N]
F_sum6	=AG57+AG66	
σ_6	=AG58/AG54	[Pa]
	=AG59/1000000	[Mpa]
Section 7		
Cross Sectional Area (A)	='Airfoil Inertia'!DP206	[m^2]
r7	=($AG$9/10)*7+$AG$7	[m]
r6	=($AG$9/10)*6+$AG$7	[m]
F_7	=$AG$4*AG62*($AG$6^2)*(((AG63^2)-(AG64^2))/2)	[N]
F_sum7	=AG65+AG74	
σ_7	=AG66/AG62	[Pa]
	=AG67/1000000	[Mpa]
Section 8		
Cross Sectional Area (A)	='Airfoil Inertia'!EH206	[m^2]
r8	=($AG$9/10)*8+$AG$7	[m]
r7	=($AG$9/10)*7+$AG$7	[m]
F_8	=$AG$4*AG70*($AG$6^2)*(((AG71^2)-(AG72^2))/2)	[N]
F_sum8	=AG73+AG82	
σ_8	=AG74/AG70	[Pa]
	=AG75/1000000	[Mpa]
Section 9		
Cross Sectional Area (A)	='Airfoil Inertia'!EZ206	[m^2]
r9	=($AG$9/10)*9+$AG$7	[m]
r8	=($AG$9/10)*8+$AG$7	[m]
F_9	=$AG$4*AG78*($AG$6^2)*(((AG79^2)-(AG80^2))/2)	[N]
F_sum9	=AG81+AG90	
σ_9	=AG82/AG78	[Pa]
	=AG83/1000000	[Mpa]
Section 10		
Cross Sectional Area (A)	='Airfoil Inertia'!FR206	[m^2]
r10	=($AG$9/10)*10+$AG$7	[m]
r9	=($AG$9/10)*9+$AG$7	[m]
F_10	=$AG$4*AG86*($AG$6^2)*(((AG87^2)-(AG88^2))/2)	[N]
F_sum10	=AG89	
σ_10	=AG90/AG86	[Pa]
	=AG91/1000000	[Mpa]

Shear Force (airfoil)		
Section 1		
I_airfoil	='Airfoil Inertia'!Q206	[m^4]
Q_airfoil	='Airfoil Inertia'!S206	[m^3]
t_airfoil	='Airfoil Inertia'!P1	[m]
τ_1	=(S19*BJ8)/(BJ7*BJ9)	[Pa]
Section 2		
I_airfoil	='Airfoil Inertia'!AH206	[m^4]
Q_airfoil	='Airfoil Inertia'!AJ206	[m^3]
t_airfoil	='Airfoil Inertia'!AF1	[m]
τ_2	=(S27*BJ13)/(BJ12*BJ14)	[Pa]
Section 3		
I_airfoil	='Airfoil Inertia'!AZ206	[m^4]
Q_airfoil	='Airfoil Inertia'!BB206	[m^3]
t_airfoil	='Airfoil Inertia'!AX1	[m]
τ_2	=(S35*BJ18)/(BJ17*BJ19)	[Pa]
Section 4		
I_airfoil	='Airfoil Inertia'!BR206	[m^4]
Q_airfoil	='Airfoil Inertia'!BT206	[m^3]
t_airfoil	='Airfoil Inertia'!BP1	[m]
τ_4	=(S43*BJ23)/(BJ22*BJ24)	[Pa]
Section 5		
I_airfoil	='Airfoil Inertia'!CJ206	[m^4]
Q_airfoil	='Airfoil Inertia'!CL206	[m^3]
t_airfoil	='Airfoil Inertia'!CH1	[m]
τ_5	=(S51*BJ28)/(BJ27*BJ29)	[Pa]
Section 6		
I_airfoil	='Airfoil Inertia'!DC206	[m^4]
Q_airfoil	='Airfoil Inertia'!DE206	[m^3]
t_airfoil	='Airfoil Inertia'!DA1	[m]
τ_6	=(S59*BJ33)/(BJ32*BJ34)	[Pa]
Section 7		
I_airfoil	='Airfoil Inertia'!DU206	[m^4]
Q_airfoil	='Airfoil Inertia'!DW206	[m^3]
t_airfoil	='Airfoil Inertia'!DS1	[m]
τ_7	=(S67*BJ38)/(BJ37*BJ39)	[Pa]
Section 8		
I_airfoil	='Airfoil Inertia'!EM206	[m^4]
Q_airfoil	='Airfoil Inertia'!EO206	[m^3]
t_airfoil	='Airfoil Inertia'!EK1	[m]
τ_8	=(S75*BJ43)/(BJ42*BJ44)	[Pa]
Section 9		
I_airfoil	='Airfoil Inertia'!FE206	[m^4]
Q_airfoil	='Airfoil Inertia'!FG206	[m^3]
t_airfoil	='Airfoil Inertia'!FC1	[m]
τ_9	=(S83*BJ48)/(BJ47*BJ49)	[Pa]
Section 10		
I_airfoil	='Airfoil Inertia'!FW206	[m^4]
Q_airfoil	='Airfoil Inertia'!FY206	[m^3]
t_airfoil	='Airfoil Inertia'!FU1	[m]
τ_10	=(S91*BJ53)/(BJ52*BJ54)	[Pa]

q_1	='Aero Model'!Z12	[N]
q_2	='Aero Model'!Z13	[N]
q_3	='Aero Model'!Z14	[N]
q_4	='Aero Model'!Z15	[N]
q_5	='Aero Model'!Z16	[N]
q_6	='Aero Model'!Z17	[N]
q_7	='Aero Model'!Z18	[N]
q_8	='Aero Model'!Z19	[N]
q_9	='Aero Model'!Z20	[N]
q_10	='Aero Model'!Z21	[N]
m_1	=(Z3*S16)*(S16/2)	[N.m.]
m_2	=(Z4*S24)*(S16+(S24/2))	[N.m.]
m_3	=(Z5*S32)*(S16+S24+(S32/2))	[N.m.]
m_4	=(Z6*S40)*(S16+S24+S32+(S40/2))	[N.m.]
m_5	=(Z7*S48)*(S16+S24+S32+S40+(S48/2))	[N.m.]
m_6	=(Z8*S56)*(S16+S24+S32+S40+S48+(S56/2))	[N.m.]
m_7	=(Z9*S64)*(S16+S24+S32+S40+S48+S56+(S64/2))	[N.m.]
m_8	=(Z10*S72)*(S16+S24+S32+S40+S48+S56+S64+(S72/2))	[N.m.]
m_9	=(Z11*S80)*(S16+S24+S32+S40+S48+S56+S64+S72+(S80/2))	[N.m.]
m_10	=(Z12*S88)*(S16+S24+S32+S40+S48+S56+S64+S72+S80+(S88/2))	[N.m.]

Max in Plane Shear Stress		
	[Pa]	[MPa]
Section 1 Max Airfoil Stress	=SQRT(((BD6/2)^2)+(BJ10^2))	=BT7/1000000
Section 1 Max Aluminium Stress	=SQRT(((BD7/2)^2)+(BN10^2))	=BT8/1000000
Section 2 Max Airfoil Stress	=SQRT(((BD9/2)^2)+(BJ20^2))	=BT9/1000000
Section 2 Max Aluminium Stress	=SQRT(((BD10/2)^2)+(BN15^2))	=BT10/1000000
Section 3 Max Airfoil Stress	=SQRT(((BD12/2)^2)+(BJ20^2))	=BT11/1000000
Section 3 Max Aluminium Stress	=SQRT(((BD13/2)^2)+(BN20^2))	=BT12/1000000
Section 4 Max Airfoil Stress	=SQRT(((BD15/2)^2)+(BJ25^2))	=BT13/1000000
Section 4 Max Aluminium Stress	=SQRT(((BD16/2)^2)+(BN25^2))	=BT14/1000000
Section 5 Max Airfoil Stress	=SQRT(((BD18/2)^2)+(BJ30^2))	=BT15/1000000
Section 5 Max Aluminium Stress	=SQRT(((BD19/2)^2)+(BN30^2))	=BT16/1000000
Section 6 Max Airfoil Stress	=SQRT(((BD21/2)^2)+(BJ35^2))	=BT17/1000000
Section 6 Max Aluminium Stress	=SQRT(((BD22/2)^2)+(BN35^2))	=BT18/1000000
Section 7 Max Airfoil Stress	=SQRT(((BD24/2)^2)+(BJ40^2))	=BT19/1000000
Section 8 Max Airfoil Stress	=SQRT(((BD27/2)^2)+(BJ45^2))	=BT20/1000000
Section 9 Max Airfoil Stress	=SQRT(((BD30/2)^2)+(BJ50^2))	=BT21/1000000
Section 10 Max Airfoil Stress	=SQRT(((BD33/2)^2)+(BJ55^2))	=BT22/1000000

RESULTS											
Normal Stress			**Pure SF**	**Centrifugal Force**			**Pure SF**	**Shear Stress**			
Section 1 Max Normal Airfoil Stress	=BF6	[MPa]	=Interface!$C$12/C5	Section 1 Centri Airfoil Stress	=AG20	[MPa]	=Interface!$C$12/H5	Section 1 Shear Airfoil Stress	=BJ10/1000000	[MPa]	
Section 2 Max Normal Airfoil Stress	=BF9	[MPa]	=Interface!$C$12/C6	Section 2 Centri Airfoil Stress	=AG28	[MPa]	=Interface!$C$12/H6	Section 2 Shear Airfoil Stress	=BJ15/1000000	[MPa]	
Section 3 Max Normal Airfoil Stress	=BF12	[MPa]	=Interface!$C$12/C7	Section 3 Centri Airfoil Stress	=AG36	[MPa]	=Interface!$C$12/H7	Section 3 Shear Airfoil Stress	=BJ20/1000000	[MPa]	
Section 4 Max Normal Airfoil Stress	=BF15	[MPa]	=Interface!$C$12/C8	Section 4 Centri Airfoil Stress	=AG44	[MPa]	=Interface!$C$12/H8	Section 4 Shear Airfoil Stress	=BJ25/1000000	[MPa]	
Section 5 Max Normal Airfoil Stress	=BF18	[MPa]	=Interface!$C$12/C9	Section 5 Centri Airfoil Stress	=AG52	[MPa]	=Interface!$C$12/H9	Section 5 Shear Airfoil Stress	=BJ30/1000000	[MPa]	
Section 6 Max Normal Airfoil Stress	=BF21	[MPa]	=Interface!$C$12/C10	Section 6 Centri Airfoil Stress	=AG60	[MPa]	=Interface!$C$12/H10	Section 6 Shear Airfoil Stress	=BJ35/1000000	[MPa]	
Section 7 Max Normal Airfoil Stress	=BF24	[MPa]	=Interface!$C$12/C11	Section 7 Centri Airfoil Stress	=AG68	[MPa]	=Interface!$C$12/H11	Section 7 Shear Airfoil Stress	=BJ40/1000000	[MPa]	
Section 8 Max Normal Airfoil Stress	=BF27	[MPa]	=Interface!$C$12/C12	Section 8 Centri Airfoil Stress	=AG76	[MPa]	=Interface!$C$12/H12	Section 8 Shear Airfoil Stress	=BJ45/1000000	[MPa]	
Section 9 Max Normal Airfoil Stress	=BF30	[MPa]	=Interface!$C$12/C13	Section 9 Centri Airfoil Stress	=AG84	[MPa]	=Interface!$C$12/H13	Section 9 Shear Airfoil Stress	=BJ50/1000000	[MPa]	
Section 10 Max Normal Airfoil Stress	=BF33	[MPa]	=Interface!$C$12/C14	Section 10 Centri Airfoil Stress	=AG92	[MPa]	=Interface!$C$12/H14	Section 10 Shear Airfoil Stress	=BJ55/1000000	[MPa]	
Normal/Centri Combined Stress			**SF**	**Shear/Centri Combined Stress**			**SF**				
Section 1 Max Airfoil Stress	=H5+C5	[MPa]	=Interface!$C$12/C17	Section 1 Max Airfoil Stress	=BU7	[MPa]	=Interface!$C$12/H17				
Section 2 Max Airfoil Stress	=H6+C6	[MPa]	=Interface!$C$12/C18	Section 2 Max Airfoil Stress	=BU9	[MPa]	=Interface!$C$12/H18				
Section 3 Max Airfoil Stress	=H7+C7	[MPa]	=Interface!$C$12/C19	Section 3 Max Airfoil Stress	=BU11	[MPa]	=Interface!$C$12/H19				
Section 4 Max Airfoil Stress	=H8+C8	[MPa]	=Interface!$C$12/C20	Section 4 Max Airfoil Stress	=BU13	[MPa]	=Interface!$C$12/H20				
Section 5 Max Airfoil Stress	=H9+C9	[MPa]	=Interface!$C$12/C21	Section 5 Max Airfoil Stress	=BU15	[MPa]	=Interface!$C$12/H21				
Section 6 Max Airfoil Stress	=H10+C10	[MPa]	=Interface!$C$12/C22	Section 6 Max Airfoil Stress	=BU17	[MPa]	=Interface!$C$12/H22				
Section 7 Max Airfoil Stress	=H11+C11	[MPa]	=Interface!$C$12/C23	Section 7 Max Airfoil Stress	=BU19	[MPa]	=Interface!$C$12/H23				
Section 8 Max Airfoil Stress	=H12+C12	[MPa]	=Interface!$C$12/C24	Section 8 Max Airfoil Stress	=BU20	[MPa]	=Interface!$C$12/H24				
Section 9 Max Airfoil Stress	=H13+C13	[MPa]	=Interface!$C$12/C25	Section 9 Max Airfoil Stress	=BU21	[MPa]	=Interface!$C$12/H25				
Section 10 Max Airfoil Stress	=H14+C14	[MPa]	=Interface!$C$12/C26	Section 10 Max Airfoil Stress	=BU22	[MPa]	=Interface!$C$12/H26				

Table 28: Model output and results

Blade Section	Unit	1	2	3	4	5	6	7	8	9	10
Chord Length	m	0.42	0.46	0.49	0.39	0.32	0.27	0.24	0.21	0.19	0.17
Pitch Angle	deg	29	21	18	14	12	9	7	6	5	4
Thrust Delivered at [2.15 m/s]	N	1.31	2.6	3.68	4.13	4.26	5.4	6.18	7.01	8.07	8.68
Torque Delivered at [2.15 m/s]	N.m.	0.37	0.48	0.12	0.37	0.97	1.58	2.35	3.25	4.00	4.66
Thrust Delivered at [17.5 m/s]	N	103.4	201.4	349.7	381.4	413.2	472.3	523.4	575.0	621.8	662.8
Torque Delivered at [17.5 m/s]	N.m.	27.7	35.4	2.7	43.7	105.7	148.5	209.2	276.2	315.5	362.3
Centrifugal Stress at [17.5 m/s]	MPa	1.55	1.46	1.31	1.41	1.44	1.39	1.27	1.07	0.79	0.44
Normal Stress at [17.5 m/s]	MPa	6.96	4.93	3.47	3.88	3.87	3.56	2.81	1.81	0.80	0.11
Shear Stress at [17.5 m/s]	MPa	0.185	0.146	0.121	0.125	0.123	0.120	0.107	0.085	0.056	0.02
Centri&Normal Stress Combined at [17.5 m/s]	MPa	8.51	6.38	4.79	5.29	5.32	4.96	4.09	2.89	1.60	0.55
Centri&Shear Stress Combined at [17.5 m/s]	MPa	3.48	2.47	1.74	1.94	1.94	1.79	1.41	0.91	0.40	0.06
Safety Factor at [17.5 m/s]	-	1.02	1.36	1.82	1.64	1.64	1.75	2.13	3.01	5.44	15.93

APPENDIX B: DETAIL DRAWINGS OF ROTOR BLADE

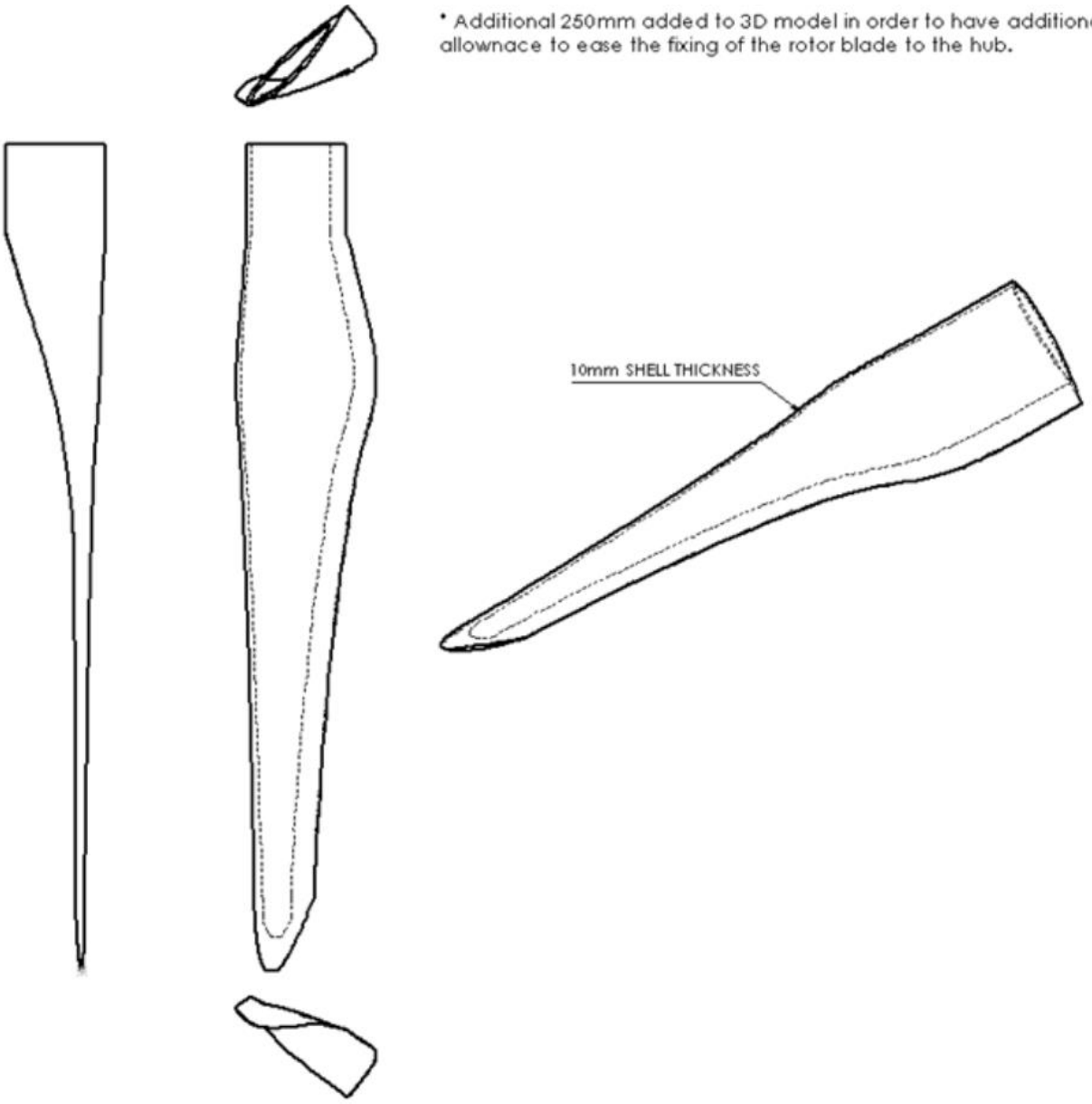

Figure 29: Additional blade illustration

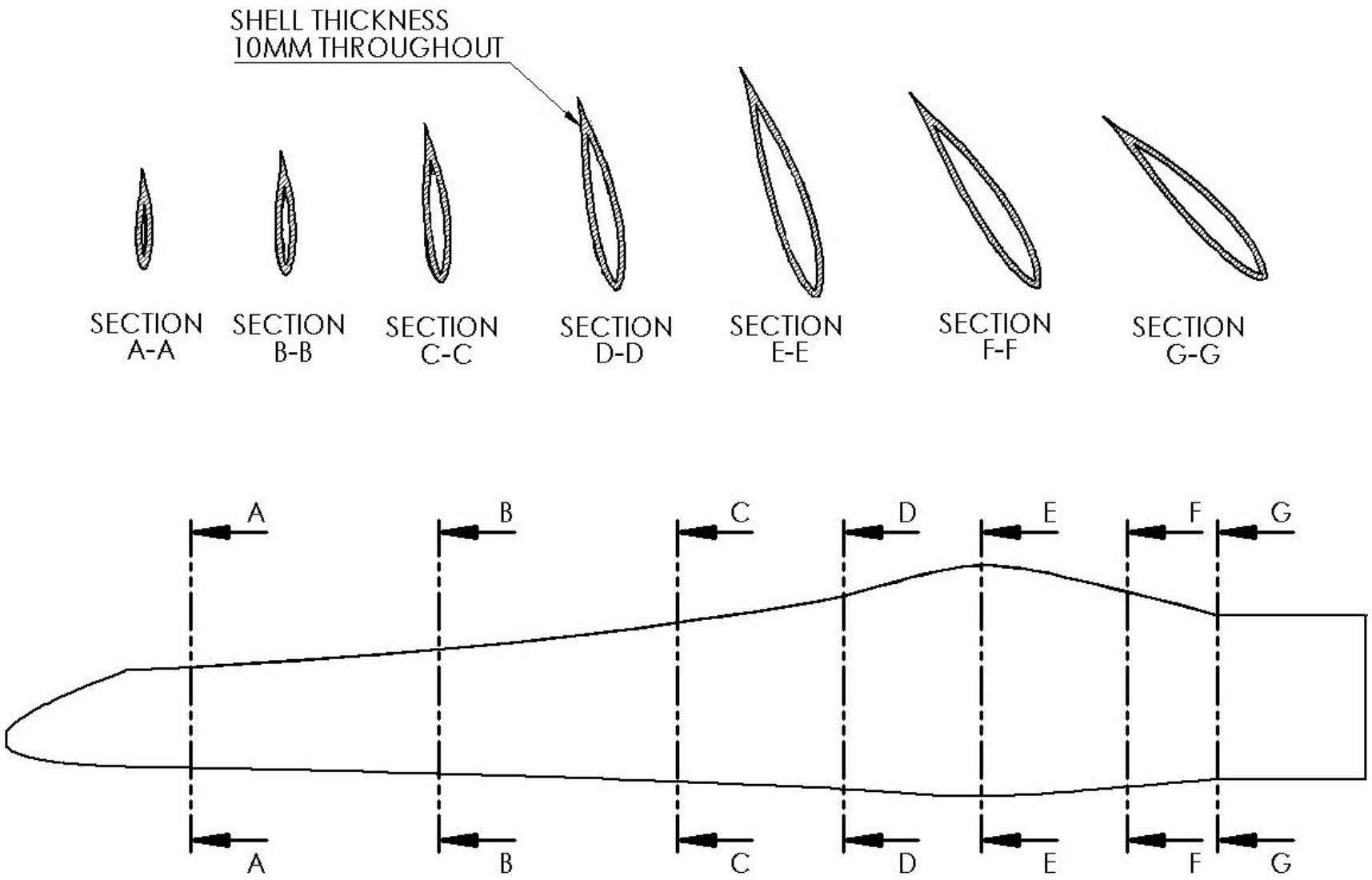

Figure 30: Illustration of uniform shell thickness as per rotational moulding